Manuscript Click here to download Manuscript renamed_55dfc.docx

Click here to view linked References

Zircon geochronology and geochemistry to constrain the youngest eruption events and magma evolution of the Mid-Miocene ignimbrite flare-up in the Pannonian Basin, eastern-central Europe.

Réka Lukács[1,2], Szabolcs Harangi[1,3], Olivier Bachmann[4], Marcel Guillong[4], Martin Danišík[5], Yannick Buret[4], Albrecht von Quadt[4], István Dunkl[6], László Fodor[7], Jakub Sliwinski[4], Ildikó Soós[1], János Szepesi[1]

[1]*MTA-ELTE Volcanology Research Group, 1117, Budapest Pázmány Péter sétány 1/C, Budapest, Hungary*

[2]*Department of Mineralogy, Geochemistry and Petrology, University of Szeged, 6722, Egyetem u. 2, Szeged, Hungary*

[3]*Department of Petrology and Geochemistry, Eötvös Loránd University, Budapest, Hungary*

[4]*Institute of Geochemistry and Petrology, Department of Earth Sciences, ETH Zürich, Clausiusstrasse 25, 8092 Zürich, Switzerland*

[5]*TIGeR/John de Laeter Centre for Isotope Research, Applied Geology, Curtin University of Technology, GPO Box U1987, Perth WA 6845, Australia*

[6]*Sedimentology & Environmental Geology, Geoscience Center, University of Göttingen, Goldschmidtstrasse 3, D-37077 Göttingen, Germany*

[7]*MTA-ELTE Geological, Geophysical and Space Science Research Group of the Hungarian Academy of Sciences, Eötvös University, 1117 Budapest Pázmány Péter sétány 1/C, Budapest, Hungary*

reka.harangi@gmail.com, Tel: +3613722500/8359, Fax: +3613722500/8007

Keywords: zircon crystallization age, eruption age, magma storage, LA-ICP-MS, (U-Th)/He, Bükkalja Volcanic Field

Abstract

A silicic ignimbrite flare-up episode occurred in the Pannonian Basin during the Miocene, coeval with the syn-extensional period in the region. It produced important correlation horizons in the regional stratigraphy; however, they lacked precise and accurate geochronology. Here, we used U-Pb (LA-ICP-MS and ID-TIMS) and (U-Th)/He dating of zircons to determine the eruption ages of the youngest stage of this volcanic activity and constrain the longevity of the magma storage in crustal reservoirs. Reliability of the U-Pb data is supported by (U-Th)/He zircon dating and magnetostratigraphic constraints.

We distinguish four eruptive phases from 15.9±0.3 Ma to 14.1±0.3 Ma, each of which possibly includes multiple eruptive events. Among these, at least two large volume eruptions (>10 km^3) occurred at 14.8±0.3 Ma (Demjén ignimbrite) and 14.1±0.3 Ma (Harsány ignimbrite). The in-situ U-Pb zircon dating show wide age ranges (up to 700 kyr) in most of the crystal-poor pyroclastic units, containing few to no xenocrysts, that implies efficient recycling of antecrysts. We propose that long-lived silicic magma reservoirs, mostly kept as high crystallinity mushes, have existed in the Pannonian Basin during the 16-14 Ma period. Small but significant differences in zircon, bulk rock and glass shard composition among units suggest the presence of spatially separated reservoirs, sometimes existing contemporaneously. Our results also better constrain the time frame of the main tectonic events that occurred in the northern Pannonian Basin: we refined the upper temporal boundary (15 Ma) of the youngest

counter clockwise block rotation and the beginning of a new deformation phase, which structurally characterised the onset of the youngest volcanic and sedimentary phase.

Keywords: zircon geochronology; zircon trace element composition; ignimbrite flare-up; silicic magma reservoir; Pannonian Basin

Introduction

Reconstructing the chronology of large explosive eruptions fed by silicic magmas and constraining the lifetime of magmatic systems are fundamental challenges in volcanic petrology (Reid and Coath 2000; Vazquez and Reid 2004; Charlier et al. 2005; Bachmann and Bergantz 2008; Wilson and Charlier 2009; Schmitt et al. 2011; Danišík et al. 2012; Gelman et al. 2013; Wotzlaw et al. 2013; 2014; 2015 Cooper and Kent 2014; Cooper et al. 2014a; Frazer et al. 2014; Simon et al. 2014). The origin and evolution of such silicic magma bodies, which either feed large volcanic eruptions or end up crystallizing as plutonic masses, still generates much debate. Silicic magma bodies could represent long-lived crystal mushes (e.g., Bachmann and Bergantz, 2004; Huber et al., 2010; Gelman et al., 2013, Cooper and Kent 2014), in which eruptible melt pods accumulate due to gravitational separation (Hildreth, 2004; Hildreth and Wilson, 2007; Shane et al., 2005; 2007; Smith et al., 2004; Bachmann and Bergantz, 2008; Deering et al., 2011; Cooper et al., 2012). Alternatively, they can form by intermittent short-lived (<10's ka) intrusive pulses of silicic magma from the mid to lower crust (Glazner et al., 2004; Zimmerer and McIntosh, 2012; Simon et al., 2014; Annen et al., 2015, Glazner et al., 2015) resulting in a multi-phase plutonic body with extended zircon crystallization, periodically re-melted by magma recharge events to form eruptible silicic pockets (Sparks et al., 1990; Simon et al., 2014).

Zircon geo- and thermochronology, combined with textural and geochemical studies, is a powerful tool to constrain eruption ages and provides insight into the interaction of melt, crystals and host rock in these magmatic systems. Zircons from silicic volcanic rocks typically show large variations in U-Pb and U-Th ages (Charlier et al., 2005; Costa, 2008; Simon et al., 2008; Cooper and Kent, 2014) indicating that prolonged crystallization and/or effective recycling and mixing before eruption could occur in the magma storage region. In this regard, however, it is important to define what the terms "magma chamber" and "magma reservoirs" mean.

A "magma chamber" as defined by Hildreth (2004) and Hildreth and Wilson (2007), is the shallow crustal part of the magmatic system where melt is present and thus, it involves both melt-dominated ("melt lens", "holding chamber" or "magma body") and the crystal-dominated zones, where melt is still present in significant amounts ("crystal mush"). In contrast, Bachmann and Bergantz (2008) confined the term "magma chamber" only to the melt-dominated (<50 vol% crystals) eruptible bodies and applied the term "magma reservoir" to what was dubbed the "magma chamber" by Hildreth and Wilson (2007). Definition of these terms is important when we discuss the lifetime of the silicic magmatic systems and in this paper we follow the nomenclature as described by Bachmann and Bergantz (2008). We use the term "magma storage" as a synonym for "magma reservoir."

Melt-dominated bodies can be formed intermittently and separately in crystal mush zones, potentially supplying volcanic eruptions. They could be assembled relatively fast (less than a few 10's ka or even faster; e.g.,

Reid and Coath, 2000; Charlier et al., 2005; Gualda et al., 2012; Simon et al., 2014) via extraction of the interstitial evolved melt fractions from the crystal mush zone and could have relatively short life-times (<50 ka; Huppert and Sparks, 1988; Sparks et al., 1990; Barboni and Schoene 2014). Charlier et al. (2005) suggested that phenocrystic zircons (we use this term here instead of autocryst as suggested by Miller et al., 2007) could characterize the melt-dominated body, i.e. the magma chamber. In contrast, the mushy magma body could have a much longer timescale (several 100 kyr) as shown by crystal-rich ignimbrites like the Fish Canyon Tuff (Bachmann et al., 2002; 2007a; Bachmann and Bergantz, 2003; Wotzlaw et al., 2013) and Kos Plateau Tuff (Bachmann et al., 2007b). These events involve the eruption of rejuvenated near-solidus crystal mush material containing dominantly antecrystic zircons which grew in different areas of the magma storage zone (Bacon and Lowenstern, 2005; Miller et al., 2007). Thus, they represent complex histories of magmatic evolution and record changes in the physiochemical condition of the surrounding magma during their growth. Intermittent mixing of crystal mushes could recycle earlier crystallized zircons and therefore, even single zircon grains can contain growth zones spanning several 100 kyr (e.g., Brown and Fletcher 1999; Harangi et al. 2015).

In this paper, we focus on the eruption chronology and the life-time of the magmatic system of the Bükkalja Volcanic Field, one of the largest Cenozoic ignimbrite flare-up periods in Europe. The silicic volcanism during the Miocene was coeval with the formation of the Pannonian Basin during the peak-extension phase (Horváth and Royden, 1981; Harangi et al., 2005; Lukács et al., 2005; Horváth et al. 2006; 2015; Harangi and Lenkey, 2007; Czuppon et al., 2012). Despite of the importance of this volcanism to the regional geotectonic history, no precise age data has been published. K/Ar data (Márton and Pécskay, 1998) suggest that the volcanism occurred between 21 and 13 Ma, however these ages have associated large uncertainties (4-14%). The volcanic products in the Bükkalja Volcanic Field remained remarkably fresh (Harangi et al. 2005), and in addition to the excellent outcrops of diverse ignimbrite products, many deep drill-cores are available from the region. Thus, their thorough investigation can help to (1) better understand the storage and eruption history of silicic magmas; (2) constrain the tectonic relationship of the magmatism (Márton and Fodor 1995; Petrik et al. 2014; 2015); (3) define key-horizons for regional correlations; and (4) promote the importance of the relatively poorly-known but significant silicic ignimbrite flare-up in central Europe.

Geological background

The Bükkalja Volcanic Field (BVF) is located in the northern part of the Carpathian-Pannonian Region, eastern-central Europe (Fig. 1). It represents the volcanic products of the Middle Miocene silicic ignimbrite flare-up episode (Harangi et al., 2005; Lukács et al., 2005; Harangi and Lenkey, 2007) that was coeval with the main lithospheric thinning and formation of the Pannonian Basin (Horváth, 1993; Horváth et al., 2006). The volcanic rocks consist of rhyolitic-dacitic unwelded and welded ignimbrites with subordinate pyroclastic fall deposits (Szakács et al., 1998; Harangi et al., 2005; Czuppon et al., 2012). Most of the ignimbrites are crystal-poor, and only the Bogács unit contains crystal-rich, strongly heterogeneous volcanic products (Czuppon et al., 2012). The pyroclastic deposits are well-preserved, providing excellent samples to examine the nature of silicic volcanism in an extensional geodynamic setting. Isotopic and trace element composition of the pumices show a gradual change with time (e.g., decreasing $^{87}Sr/^{86}Sr$ and Th/Nb ratios), possibly due to the contemporaneous crustal thinning that would increase the proportion of mantle component in the magmas (Harangi and Lenkey, 2007).

The silicic pyroclastic rocks were formed during recurring phases of volcanic activity between 21 and 13 Ma (Szabó et al, 1992; Márton and Pécskay, 1998; Pécskay et al., 2006). The K/Ar geochronology (determined mainly on bulk rock or biotite samples) provides largely overlapping eruption ages due to the large uncertainties, and therefore does not allow discrimination of different volcanic stages (Márton and Pécskay, 1998). Furthermore, K/Ar ages obtained from biotite on such samples could also be subject to inaccuracies due to excess ^{40}Ar (see Bachmann et al. 2010 and Hora et al. 2010).

Two significant block-rotation phases (at 18.5-17.5 Ma and 16.0-14.5 Ma) were suggested to have occurred based on palaeomagnetic analyses of the volcanic rocks of BVF (Márton and Pécskay, 1998; Márton et al., 2007) and may be representative of regional deformation in the Northern Pannonian Basin (Márton and Fodor, 1995). Combining the published K/Ar and palaeomagnetic data, Márton and Pécskay (1998) distinguished three main eruption periods in the BVF: 21.0-18.5 Ma, 17.5-16.0 Ma and 14.5-13.5 Ma (Fig. 1), which were correlated with the regionally-distributed pyroclastic rocks of similar age in the Pannonian Basin. These three eruption periods form three distinct tuff horizons (i.e., the "lower rhyolite tuff", "middle rhyolite tuff", "upper rhyolite tuff", respectively; Hámor et al., 2001). The volcanic eruptions produced large volume ignimbrites, occasionally exceeding several hundred meters in thickness (Lukács et al., 2010). Although the eruptive volume of these events is consistent with caldera-forming eruptions, no eruptive centres have been successfully identified.

This silicic volcanism appears to have produced one of the most voluminous volcanic deposits in Europe during the Miocene. The volcanic rocks of this long-lasting volcanism were subsequently covered by younger (Upper Miocene) sediments as a result of the major thermal subsidence which followed the prolonged rifting phase in the Pannonian Basin (Horváth et al. 2006; 2015; Danišík et al. 2015). Due to post-Miocene (neotectonic) exhumation, tilting and denudation (Dunkl et al. 1994), the foreland of the uplifted Bükk Mountains. (called Bükkalja) provides an excellent target area to study these volcanic sequences. It exposes the volcanic products of almost the entire ignimbrite flare-up episode in a gently southward-tilted position. In addition, many deep boreholes located to the south and east of Bükkalja reveal vast amount of volcanoclastic suites, occasionally over 1 km thick (e.g., Zelenka et al. 2004; Széky-Fux et al. 2007; Lukács et al. 2010).

Samples

In this work, we focus on deposits of the youngest volcanic period of the BVF which has been previously dated as 14.5-13.5 Ma by K/Ar data (Márton and Pécskay 1998; Fig. 1). We collected samples from outcrops and drill-cores located 4-15 km south of the sampling locations, which provide continuous stratigraphic sequences of successive volcanic units (Figs. 1 and 2). The continuous stratigraphic sequence of Tibolddaróc outcrop provides the best-exposed section, where alternation of primary and secondary volcaniclastics suggests quiescent periods between the eruptive episodes (Fig. 2, Lukács et al. 2007; Harangi and Lukács 2009).

The lowest part of the section is called Bogács Unit (Td-M), which is a >30 m thick crystal-rich pyroclastic flow deposit characterized by mixed juvenile clasts, previously interpreted as resulting from the evacuation of some crystal mush portions from the magma reservoir (Czuppon et al., 2012). It belongs to the volcanic period between 17.5 and 16 Ma (Márton and Pécskay, 1998), and is usually referred to as "middle rhyolite tuff" (Hámor et al., 2001). This unit is easily distinguished from the subsequent younger unit (the so-called "upper rhyolite tuff"; Hámor et al., 2001), which is the focus of the present study. Samples of 5 primary volcanic layers

(from oldest to youngest: Td-J; Td-H; Td-F; Td-E; Td-A) above the Bogács Unit (Td-M) were used for detailed zircon geochronology (Fig. 2). All samples are crystal-poor rhyolites containing remarkably fresh glasses and phenocrysts of plagioclase, quartz +/- biotite and rarely sanidine. The Td-A unit was described in detail by Lukács et al. (2007; 2009) and denoted as Harsány Ignimbrite. K/Ar dating of biotites yield an eruption age of 13.35±1.01 Ma, which is one of the youngest in the BVF. In addition, we collected two samples from the western part of the BVF (Fig.1), which are thought to be the youngest volcanic products on the basis of palaeomagnetic and K/Ar data (Márton and Pécskay, 1998; Márton et al. 2007). Sample DEMNE-1 is from the Demjén-Nagyeresztvény quarry southwest of BVF, and FN1 is from the Felnémet quarry northwest of BVF. They both represent unwelded to slightly welded pyroclastic flow deposits with phenocrysts assemblages of quartz, plagioclase, biotite and amphibole. Trace element compositions of the glass shards from the DEMNE-1 locality show a distinct character among the BVF ignimbrites (Harangi et al., 2005), but the DEMNE ignimbrite was thought to be formed roughly coeval with the Harsány ignimbrite.

We collected samples from the Szv-3 (Szekrény-völgy) and Mn-2 (Mezőnyárád) drill-cores (samples named Szv3-1 and 2; Mn2-1 and 2). In these drill-cores, the Bogács Unit was clearly identified and we focus on the volcanic succession above this level (Fig. 3), to match outcrop samples. The 601 m long Szv-3 borehole was drilled near the southern border of the exposed part of BVF close to Tard village, while the 2480 m long Mn-2 borehole was drilled ~12 km SE of the BVF located within the Vatta-Maklár trough close to its southern margin (Fig. 1). Sample Szv3-1 is from the 200.3-204 m interval and represents a homogeneous pumiceous pyroclastic flow deposit at the top of the volcanic series (from 157 to ~204 m). Beneath ~237 m, the size distribution of the pyroclastics changes without a clear unconformity. Szv3-2 is a characteristic sample of the interval 243.7–263 m and is a lapilli-bearing tuff with <1 cm pumices. Mn2-1 (1183.7-1188.9 m), and Mn2-2 (1263-1268 m) are taken from the middle and lower part of the pyroclastic unit defined above the recognized Bogács Unit in the borehole Mn-2 (Fig. 3). They are both compacted and variably altered pumice-bearing lapilli tuffs. Mn2-2 sample looks less fresh and contains charcoal. All borehole samples have rhyolitic pumices with quartz, plagioclase, biotite phenocrysts and altered glass shards (with devitrification, secondary clay mineralization).

Methods

Zircon crystals were separated from juvenile clasts in Td-A and from bulk rock tuff or lapilli tuff samples everywhere else. We separated the zircon crystals by standard gravity and magnetic methods from the 63-125 µm size fractions. All samples were investigated using optical microscopy, cathodoluminescence (CL) and back-scattered electron (BSE) imaging.

Zircon geochronology

The majority of the U-Pb geochronological data were obtained by LA-ICP-MS at ETH Zürich. These were coupled with (U-Th)/He analyses of 5 samples at the University of Waikato (New Zealand) and by U-Pb ID-TIMS dating of one sample at ETH Zürich. In order to minimize the effects of lead loss, chemical abrasion (CA; Mattinson 2005) was carried out prior to zircon dissolution for the ID-TIMS analysis and in the case of two samples (Td-A_CA, Td-H_CA) which were afterward analyzed by LA-ICP-MS. Detailed methodology of the CA and ID-TIMS analyses can be found in the Electronic Supplementary Material (Online Resource 1). All U-Pb geochronological data were corrected for Th disequilibrium using the equation of Schaerer (1984). For the

fractionation factor ($f_{Th/U}$), the Th/U in the melt was averaged from LA-ICP-MS analyses of glass published in Harangi et al. (2005) or calculated from the bulk rock analyses (Lukács et al. 2009 and this study). The Th/U melt values are between 2.5 and 4.1. Calculating the in situ $^{206}Pb/^{238}U$ age data using the two end-member Th/U melt ratios, the data differ by 10,000 years. As this is well below the error range of the LA-ICP-MS age data, we used the ratio 3 for all samples. Propagating the errors from the maximum errors of Th/U_{melt} determination will not significantly change the error of the $^{206}Pb/^{238}U$ age (i.e. only in the 4th decimal, which is below 10,000 years). Th/U ratios of dated zircons were either directly measured (LA-ICP-MS) or deduced from measured $^{206}Pb/^{208}Pb$ ratios (ID-TIMS), assuming concordance. In the ID-TIMS age calculations, we used also the melt Th/U=3 ratio following the published glass data (Harangi et al. 2005).

We conducted at least 50 spot analyses for each sample with a Resonetics Resolution 155 ablation system using a 193 nm excimer laser coupled to a Thermo Element XR SF-ICP-MS. The full details of analytical conditions are similar to Guillong et al. (2014) and summarized in Online Resource 1. Analyses involved a spot size of 30 µm with a repetition rate of 5 Hz, energy density of ~2 J cm^{-2} and ablation duration of 40 s after 5 cleaning pulses and 9 s of gas blank acquisition. GJ-1 reference zircon (Jackson et al. 2004) was used as a primary standard, while Plešovice, Zircon 91500, Temora2 and OD-3 were measured as secondary standards for quality control (Sláma et al. 2008; Wiedenbeck et al. 1995; Black et al. 2004; Iwano et al. 2013, respectively). For data reduction we used IOLITE 2.5 (Paton et al. 2010; 2011) paired with VizualAge (Petrus and Kamber 2012) software. We did not apply a common Pb correction. With the help of VizualAge and live concordia diagram the integration intervals were (when possible) set to exclude the common Pb contaminated signal intervals. The data were filtered according to their U contents (<5,000,000 cps, SEM/analog counting switchover), discordance ([($^{207}Pb/^{235}U$Age) – ($^{206}Pb/^{238}U$Age)] / ($^{207}Pb/^{235}U$Age) <10%) and integration length (min. 5 s). In order to estimate the effects of possible lead loss (von Quadt et al. 2014), two samples were analyzed both with and without CA. During the CA measurements, chemically-abraded GJ-1 (GJ-1_CA) and reference zircons (Temora2_CA, 91500_CA, OD-3_CA) were used as primary and secondary standards to maintain similar ablation behavior of the unknowns and reference materials (Marillo-Sialer et al. 2014).

(U–Th)/He dating of zircons was conducted at the University of Waikato (New Zealand) following the protocols described in Danišík et al. (2012). Zircon crystals were hand-picked following the recommendation of Farley (2002). Selected crystals were characterized by euhedral shape, octagonal or tetragonal prismatic morphology with two pyramidal terminations, and the diameter of >65 µm. The crystals were then photographed, measured for physical dimensions and loaded in Nb microtubes. ^{4}He was extracted at ~1,250°C under ultra-high vacuum using a diode laser and measured by isotope dilution on a Pfeiffer Prisma QMS-200 mass spectrometer. A "re-extract" was run after each sample to verify complete outgassing of the crystals. He gas data were corrected for blank, determined by heating empty Nb tubes using the same procedure. After the ^{4}He measurements, tubes containing the crystals were retrieved from the laser cell, spiked with ^{235}U and ^{230}Th and dissolved in Parr bombs using HF and HCl (Evans et al. 2005). Sample, blank, and spiked standard solutions were analyzed by isotope dilution for ^{238}U and ^{232}Th, and by external calibration for ^{147}Sm on a PerkinElmer SCIEX ELAN DRC II ICP-MS. The total analytical uncertainty (TAU) was calculated by quadratic addition for He and weighted uncertainties on U, Th, Sm and He measurements, and is typically <5% (1σ). The raw zircon (U–Th)/He ages were corrected for alpha ejection (Ft correction: "Fraction of total"; after Farley et al. 1996), whereby a homogenous distribution of U, Th and Sm was assumed for the crystals. Replicates with associated uncertainties were used to calculate the

geometric mean and error-weighted standard deviation as representative numbers for each sample. Replicate analyses of Fish Canyon Tuff zircon (n=21) measured over the period of this study as internal standards yielded mean (U–Th)/He age of 28.4±0.8 Ma, which is in excellent agreement with the reference (U–Th)/He age of 28.3±1.3 Ma (Reiners 2005). We performed (U-Th)/He zircon age dating on 5 samples collected from the Td-H and Td-A units and from the Szv3-1, Mn2-1 and Mn2-2 drill cores (averages of 6-7 zircons per sample; see Table 3). All samples were collected from the lower central parts of the units in order to minimize the effect of post-depositional reheating by subsequent eruptions.

Zircon and bulk rock geochemistry

Trace element abundances were acquired at ETH Zurich using the same LA-ICP-MS system as for U-Pb analyses. In two sessions, we analysed trace elements and U-Pb ages simultaneously. We performed the analyses using 30 µm spot size, 5 Hz repetition rate, energy density (fluence) = 2.0 J cm^{-2} and 20 s (trace elements only) or 40 s (analyses coupled with geochronology) ablation time. The primary standard was NIST610 and Zircon 91500 was used for quality control. We analysed Si, REE, Y, Hf, P, Nb, Ta, U, Th in all samples and Zr, Ti in three samples. Either Al, Rb, Ba, Ca, Fe or Al, Sr were measured for monitoring glass, apatite and iron oxide inclusions. Si was used as internal standard for data reduction done by SILLS (Guillong et al. 2008). The trace element spots were oriented as close to the geochronological spots as possible. Therefore, the trace element data were coupled with the approximate ages (see Online Resource 5). Zircons from all studied units except for Td-F were analysed for in-situ trace element contents by LA-ICP-MS (results in Online Resource 3). The two chemically abraded samples were also measured. The HF leaching removed glass attached and the open glass inclusions, however, these zircons do not show significant compositional difference compared with the non-abraded ones.

Major and trace element compositions of the bulk rocks were analysed at the ACME Labs (Canada; http://www.acmelab.com/). Major and minor elements were determined by ICP-emission spectrometry, whereas trace elements were analysed by ICP-MS following a lithium borate fusion and dilute acid digestion (data in Online Resource 4). Duplicate sample analysis and internal standards were used to check the reliability of the results

Results

Zircon textures

Zircons can be broadly divided into elongated and stumpy habits (cf. Online Resource 1), all of which have magmatic textures, i.e. oscillatory and frequently sector zoning. They commonly contain melt and apatite inclusions. Zircons from Td-J, Td-H, DEMNE-1 and FN1 localities are stumpy with average aspect ratios ranging between 1.8 and 4.5 (Fig. 5). These zircons show wide, well-developed oscillatory zoned rims. Td-A (Fig. 4), Td-E, Szv-3-1, Mn-2-1 have more zircons with large aspect ratios (>5; although often only their broken fragments remained after separation). Well-developed, broad oscillatory zoned rims are less common in these zircons. In contrast, Szv-3-2, Mn-2-2 samples have more stumpy zircons. CL imaging of polished zircons reveals that texturally distinct cores with resorption surfaces and, resorption surfaces within the oscillatory zoned rims can be found in most of the samples. Zircons of Td-F sample show a bimodal character, i.e. they involve both narrow

(aspect ratios >4) and stumpy crystals. Zircons with large aspect ratios are more homogeneous in cathodoluminescence and are relatively darker than the stumpy zircons.

U-Pb geochronology

Precision and accuracy of LA-ICP-MS measurements

We consider only $^{206}Pb/^{238}U$ ages for the interpretation of the samples, because of the lower intensities of ^{207}Pb and ^{208}Pb and the larger influence from small amounts of common Pb on the $^{207}Pb/^{235}U$ and $^{208}Pb/^{232}Th$ ages. The accuracy of the measurements can be evaluated from the measured secondary standards. We analysed samples in six sessions along with routinely-used zircon reference materials (Plešovice, Temora and 91500), whereas in two sessions we used a younger reference materials (OD-3) with age comparable to our samples (~33 Ma). In addition, we analysed in one run two zircon sets after chemically abrasion along with CA zircon reference materials (OD-3_CA, Temora2_CA, 91500_CA). The mean age of the secondary standards during the sessions agree well with the published ID-TIMS reference values: Plešovice: 336.46±0.52 Ma (MSWD=2.1, n=65 in 6 sessions), ref. age: 337.13±0.37 Ma of Sláma et al. (2008); Temora2: 417.36±0.79 Ma (MSWD=2.8, n=74 in 7 sessions), ref. age: 416.8±1.3 Ma of Black et al. (2004); zircon 91500: 1060.6±1.5 Ma (MSWD=1.7, n=72 in 7 sessions), ref. age: 1065±2 Ma of Wiedenbeck et al. (1995). The younger OD-3 standard (Iwano et al. 2013) gave 32.72±0.16 Ma weighted mean age (MSWD=3.2, n=33 in 3 sessions) that fits with the reference value of 32.853±0.016 Ma (ID-TIMS) and an overall weighted average age of 33.0±0.1 Ma (Iwano et al. 2013). Precision of these SRMs was found to be between 0.2% and 1.5% 2-standard-error (2se) for 7-13 replicate analyses and between 0.53% and 2.3% (2se) on individual point analyses. In two sessions, when coupled with trace element measurements, the 2se are systematically higher by ~10-30% due to less replicate measurements. The MSWD values obtained for the secondary standards are less than 5. All data can be found in the Online Resource 2 following the guidelines suggested by the Earthtime initiative (http://cirdles.org/LA-ICP-MS_Data_Handling).

Results of in-situ zircon dating

More than 750 individual zircon analyses from 11 samples were dated by LA-ICP-MS to better constrain the youngest eruption events and get insights into the magma evolution. Results are shown in Figures 6 and 7 and the full dataset is in the Online Resource 2. The number of individual age data in the suites after filtering, range from 27-51 per samples with the exception of Td-J, Td-F and Td-E (Table 1). The zircons from these three units (especially the ones of Td-E) have unusually high U concentrations; hence, a higher proportion (40-55%) of age data was discarded. In order to improve the representativeness we included measurements with higher U count rates, in case of Td-E.

$^{206}Pb/^{238}U$ dates of the 11 samples are sorted by their values (from oldest to youngest) and the majority of data spans from ~18 to ~14 Ma (Figs. 6 and 7). We have found two zircon cores with Proterozoic ages (Td-F-Grain27-41: 617±6 Ma; FN1-Grain34-43: 580±7 Ma), these dates were not used in the age calculations and are not shown in Figs. 6 and 7. Uncertainties of the individual zircon analyses are given as 2se and are usually between 1-3 % relative standard error (rse; average rse=1.5%). Zircon dates of Td-H, FN-1 and the chemically abraded

samples (Td-H_CA, Td-A_CA) have systematically higher 2se (average rse=2-2.5%) by ~40-50% as a result of the different measurement setups (including trace elements). Isoplot v3.75 (Ludwig 2012) was used to calculate the weighted means (Table 1) and UNMIX ages, which is based on the methods of Sambridge and Compston (1994) (Figs. 6 and 7). The weighted mean ages for the suite of zircons are in the range of 16.32±0.13 Ma (Td-J) to 14.19 ±0.12 Ma (Szv3-1), accompanied with MSWD (mean standard weighted deviates) values ranging from 2.3 to 24 (not calculated for Td-F). Based on high MSWD values, the spread of single concordant zircon dates exceeds the analytical scatter in most of the samples (Table 1). Therefore, the weighted mean ages have little geological meaning. The UNMIX function was used to further evaluate the age results and calculate statistically distinguishable age populations (assuming Gaussian distributions for each) for samples having individual dates that overlap within error, exemplified in sample Td-F (Figs. 6 and 7). Differences between the UNMIX age populations within one sample range from 300 kyr to 2.67 Myr. The individual zircon analyses from a single sample give either continuous or partly continuous age ranges, which cover 300 kyr to 700 kyr timespans. In contrast to von Quadt et al. (2014), no differences between the chemically abraded and non-abraded zircons were found, indicating that the accuracy of the obtained in-situ zircon dates was not affected by post crystallisation Pb loss.

Six zircon grains of sample Td-A were measured by ID-TIMS and gave an average age of 14.408±0.018 Ma (Table 2), which is in excellent agreement with the weighted mean age value of 14.37±0.10 Ma measured by LA-ICP-MS (Table 1). This agreement indicates the accuracy of our LA-ICP-MS measurements. Notably, the ID-TIMS age has an MSWD of 7.5, indicating that it cannot be used as a single population in the statistical sense. The same logic applies to the LA-ICP-MS data (MSWD is 11.5), confirming that the wide variation of the LA-ICP-MS spot-ages could reflect "geological" scatter as opposed to analytical uncertainty.

(U-Th)/He geochronology

The samples from the Tibolddaróc section yield ages of 14.63±0.61 Ma (Td-H) and 14.27±0.59 Ma (Td-A) Ft-corrected weighted mean ages, the errors (in 1 sigma confidence) on each measurements are 5.6-5.7% and 5.4%-5.6%, respectively. The youngest sample from Szv-3 borehole (Szv3-1) yielded 14.19±0.60 Ma, while the Mn2-1 sample gave 14.45±0.66 Ma Ft-corrected weighted mean ages, the errors (1σ) on measurements are 5.4%-5.7% and 5.5-5.8%, respectively. These ages are in good agreement with the in-situ U-Pb age results. Zircons from the Mn2-2 sample yield much younger and inhomogeneous ages ranging between 6.8-14.2 Ma with similar (5.5%) errors. These ages of Mn2-2, which represents the 1263-1268 m interval of the drill core suggest partial resetting after deposition.

Zircon geochemistry

Overall, trace element contents in the analysed zircons show significant variability and distinct trends among (and sometimes within) units. Hafnium concentrations range from 7000 to 12200 ppm (Fig. 8; more figures are presented in the Online Resource 5.) This wide range is particularly obvious in Td-A and the Szv3-1 zircons, whereas the other samples have a more restricted Hf range, particularly those from the DEMNE-1 and FN-1 (Hf = 9200-11200 ppm). The Hf concentration is correlated with the Th/U ratio (which ranges from 0.2 to 1.0) except

for samples where more restricted compositional variations were found. The Eu anomaly (Eu/Eu*) ranges from 0.08 to 0.45, and shows a negative correlation with the Hf content (Fig. 8). Positive correlation is found between U, Th/U and Y, with distinct trends observed even in single samples (Fig. 10). The Y content has a wide range (300-5500 ppm), although there are samples where zircons have more restricted Y content (300-2000 ppm).

Titanium (only measured in Td-J, Td-H and Td-A) shows a negative correlation with Hf in the Td-A zircons and in some of the Td-J zircons, whereas the Td-H zircons show a bimodal Ti distribution within a narrow range (9000-10200 ppm) of Hf concentrations. The Ti content ranges from 3 to 9 ppm (limits of detection are <2.7 ppm), which is similar to that found in the zircons of Bishop Tuff (Chamberlain et al. 2014). Due to the lack of appropriate oxide minerals, it is difficult to constrain the $aTiO_2$. However, we have found mostly ilmenite as FeTi-oxide phase, thus we can set arbitrary the $aTiO_2$=0.7. This corresponds to the upper estimate of the TiO_2 activity in the magma for the Bishop Tuff (Ghiorso and Gualda 2013; Chamberlain et al. 2014). Using this value, we obtained crystallization temperatures ranging from 650 to 760 °C at $aSiO_2$=1 (Ferry and Watson 2007) for the BVF zircons (Fig. 9). Decreasing the $aTiO_2$ value yields higher temperatures, although at the Ti concentration range of the BVF zircons, only subtle changes can be observed between $aTiO_2$=0.65 and 0.8, a reasonable range for the Bükkalja silicic magmas. Significantly higher temperatures are only obtained at $aTiO_2$<0.6.

Based on the compositional characteristics of the zircons (Figs. 8 and 10) and Online Resource 5), two groups can be clearly distinguished within the studied BVF samples. Both groups contain zircons with similar and coherent chemical characteristics (Fig. 8. and additional plots included in the Online Resource 5). Restricted chemical variation (e.g., in Hf, Y, Nb, P) is found in the samples Td-H, DEMNE-1 and FN-1 (denoted as Group-1), whereas the zircons of Td-A, Td-E and Szv3-1 samples (denoted as Group-2) show typically large compositional variation. There is a strong correlation between Yb/Gd ratio and P content in the Group-1 zircons, whereas no such relationship can be observed in the zircons of Group-2. The Group-1 zircons are characterized by significantly lower Y (<1800 ppm), Nb (<4 ppm) contents and lower Nb/Ta ratios (<2.7) than the Group-2 zircons. In addition, a bimodality in Yb/Gd, Eu/Eu* and Ti can be recognized at the same Hf and Th/U values in the Group-1 samples. These geochemical features cannot be explained by the effect of sector zoning. According to Chamberlain et al. (2014) and Cooper et al. (2014), Y concentrations and Eu anomaly is not affected by this type of zoning, and neither the Eu/Eu* nor the Y concentration show systematic variation in such zircons. Furthermore, we have not observed this bimodality in single zircon grains.

The additional samples (Td-J, Szv3-2 and the two Mn2 samples) cannot be classified unambiguously into either main groups, although Szv3-2 resemble rather the Group-2, while the two Mn-2 samples are akin rather to the Group-1 samples. Compositionally, the Td-J zircons share some key-features with those of the Group-1 zircons, but there are a few grains, which have strikingly different chemical character.

Bulk rock geochemistry

The variability of zircon geochemistry is consistent with the distinct bulk rock compositional characteristics of the studied pyroclastic units. Fresh pumices and bulk tuff samples (in case of fine-grained pyroclastic samples such as Td-H) were analysed from selected pyroclastic layers of the Tibolddaróc section and from the Nagyeresztvény quarry, Demjén (sample DEMNE-1). The Td-H tuff unit and pumices from Demjén are rhyodacites, whereas the others are rhyolites (SiO_2=69.5-76 wt%; K_2O=4.5-5.5 wt%; K_2O/Na_2O=1.8-3.0; Fig. 11).

The Group-2 and Group-1 groups distinguished based on zircon trace element composition show significantly different bulk rock chemistry what is consistent also with the *in situ* trace element signatures of the glass shards (Harangi et al. 2015). The Td-H tuff and the Demjén pumices are characterized by higher Th/Y, Nb/Y and Zr/Nb ratios as well as distinct Eu/Eu* ratios from those of the Group-2 deposits (Fig. 11). In the latter one, the Td-F, Td-E and Td-A pumices show clear compositional similarities. The distinct compositional character of the two groups is corroborated by the very different rare earth element patterns as well (Fig. 11b).

Discussion

Interpretation of zircon ages

In-situ analyses (e.g., LA-ICP-MS, SIMS or SHRIMP dating) are powerful tools for zircon dating since timescales of crystallization are expected to be better constrained by such methods than by bulk zircon dating (ID-TIMS; e.g. Compston et al. 1984; Williams 1998; Košler and Sylvester 2003; Davis et al. 2003; Nemchin et al. 2013) when there is intra-crystal age zonation, although the precision of spot analyses is almost an order of magnitude lower than ID-TIMS measurements (e.g. Nemchin et al. 2013; Mills 2012). Each single *in-situ* LA-ICP-MS U-Pb age determined by our instrumental settings represents a circular area of 30 μm diameter and a depth of ~15 μm. Zircons are usually ≤100 μm in width and have oscillatory zoning with or without distinct cores (CL images in Figs. 4 and 5 and in the Online Resource 1). Most of the spot analyses were performed on the zircon tips in order to obtain the youngest possible crystallization age. Several analyses were also conducted on interior zones. As the analysed areas cover several growth zones and often incorporates core regions, the obtained zircon dates represent a mixture of multiple age domains, either from successive crystal zones or even xenocrystic cores with younger rims (e.g., Sambridge and Compston 1994). It follows that the intra-sample range of the obtained U-Pb zircon spot dates should be similar, but generally smaller than the real crystallization age interval. In four data points, significantly older ages were obtained at the rim than at the core. This could be explained by 3D effects of oblique sectioning of the crystal, where old core occurred immediately underneath the rim part.

Most samples of the BVF exhibit a large range in U-Pb zircon dates which cannot be explained by analytical scatter as shown by large MSWD values (Table 1). Temporal heterogeneities in the zircon dates may result from a number of processes: (1) Pb loss; (2) common-Pb incorporation from the inclusions; (3) presence of older xenocrysts or xenocrystic cores (xenocrysts = foreign to the magmatic system; Miller et al. 2007); and (4) prolonged crystallization of zircons in the magma reservoir (i.e., mixture of co-magmatic phenocrysts and antecrysts; Miller et al. 2007). Contrary to the results of von Quadt et al. (2014), significant Pb loss in BVF samples can be ruled out since the Td-H and Td-A samples yielded exactly range in zircon dates with and without CA of the zircons (Fig. 6). The effect of common-Pb is minimized by integration interval selection and the discordance discard criterion. Explosive eruptions can remobilize older country rocks, the solidified part of the feeding channels or can even involve older tephras from the surface. Furthermore, xenocrystic zircon cores or crystals can be found in magmas that partly or wholly originated from the crust (e.g., Vazquez and Reid 2002; Charlier et al. 2005; Wilson and Charlier 2009; Bachmann et al. 2010; Aydar et al. 2012; Paquette and Le Pennec 2012; Frazer et al. 2014).

In the BVF samples, only a few xenocrystic zircons were recognised based on their distinctly older ages (shown in the probability density plots as much older age groups in Figs. 6-7 and even Proterozoic crystal cores). A clear multimodal age spectrum is observed only in the sample Td-F (Fig. 6), which is coupled with different zircon textures (i.e. the younger group comprises mainly elongated zircon habits while the older one contains mainly stumpy zircons). The 33 zircon dates of this unit have the largest variation (Fig. 6). The two largest age populations of this variation, calculated by the Isoplot UNMIX function, have mean ages of 14.70±0.05 Ma (2se) and 17.36±0.09 Ma (2se) respectively (relative misfit=0.16). The MSWD values of the weighted mean ages of the two age populations, comprising 62% and 38% of the data, are 14 and 6.6, respectively. Thus, the younger age population can be interpreted as representing the zircon phenocryst and antecryst population, while the zircons with the older ages could have derived from an older volcanic formation and thus can be regarded as xenocrystic (i.e., not directly recycled from a melt-bearing mush). We did not find any zircon grains which contain U-Pb dates from both populations, which indicates that the two zircon populations were probably mechanically mixed. In the other samples the mechanical mixing during eruption or the pyroclastic-flow deposition can be ruled out, supported by the fact that the intra-grain heterogeneities overlap with age range between grains (diagrams in Online Resource 1). Furthermore, we also stress that we obtained a significant spread in zircon dates from the Td-A sample, where zircons were separated from pumice clasts (as opposed to bulk tuff samples), limiting the risk of contamination. Hence, apart from the few zircon xenocrysts, the BVF samples can be characterized primarily by phenocrystic and antecrystic zircons showing wide and probably non-Gaussian age distributions. This allows us to infer the lifetime of zircon-saturated magmas in the system (e.g. Miller et al. 2007; Zimmerer and McIntosh 2012).

UNMIX age populations do not necessarily yield peak crystallization ages, as these ages depend on spot distribution, but we can use them to gain a first-order estimate of the timescales of the magmatic system. Taking only the continuous age ranges of the samples, the difference between the UNMIX age populations ranges from 300 kyr to ~700 kyr. These ages could be considered as the minimum lifetime of zircon-bearing, silicic magmas, in agreement with many other volcanic systems worldwide (Brown and Fletcher 1999; Charlier et al. 2005; Bachmann et al. 2007a; 2007b; Cooper et al. 2014; Cooper and Kent 2014).

Constraints on the eruption ages

Eruption ages of silicic volcanic rocks can be constrained by zircon geochronology in several ways. (U-Th)/He zircon dating provides a powerful tool for this purpose, because the closure temperature for He diffusion is about 150-220ºC for zircons (Reiners et al. 2004; Guenthner et al. 2013). Thus, the obtained ages should correspond to the eruption ages, assuming that no post-depositional reheating occurred. Corrections for alpha-ejection are required which can be obtained from morphometric analysis (Farley et al. 1996). This method was successfully used to reproduce the eruption age of the Fish Canyon Tuff and other Tertiary volcanic rocks (Reiners et al. 2002; Tagami et al. 2003; Reiners 2005; Hurai et al. 2013) and for eruption age determinations of Quaternary volcanic events (e.g. Schmitt et al. 2006; 2010; Danišík et al. 2012; Gebauer et al. 2014; Harangi et al. 2015).

As discussed above, zircon exhibit protracted growth (> 100 kys) in our samples, as well as in many other volcanic products worldwide (e.g., Brown and Fletcher 1999; Bachmann et al. 2007a; 2007b; Gelman et al. 2013; Wotzlaw et al. 2013; Klemetti and Clynne 2014; Harangi et al. 2015), making it difficult to determine the eruption age. However, the youngest U-Pb zircon dates obtained by U-Pb dating of zircons can be used to constrain the

eruption age as demonstrated by numerous studies (e.g. Charlier et al. 2005; Zimmerer and McIntosh 2012; Guillong et al. 2014), which have shown that the youngest zircon dates and age populations are usually in good agreement with the $^{40}Ar/^{39}Ar$ ages. In plutonic systems, Schaltegger et al. (2009), Memeti et al. (2010) and Schoene et al. (2012) suggested that the youngest zircon fraction in ID-TIMS bulk zircon dating should be used to approach the pluton formation, i.e., final solidification age, particularly in the case of wider age range (indicated by higher MSWD value) of samples. We followed these considerations here and used the age of the youngest UNMIX age as the statistically definable youngest crystallization age population to approach the eruption date.

The calculated 2se uncertainties of the youngest age groups (Table 4) are in the range of ca. 40 kyr to 100 kyr (<0.6% rse), which does not consider several sources of external systematic errors (Gehrels et al. 2008; Paton et al. 2010). These are (1) the uncertainties in the decay constants for ^{238}U (0.16%; Jaffey et al. 1971); (2) in the age of the primary standard (GJ-1) used for corrections (~1% estimated varitation); (3) average uncertainty of the corrections (estimated by the uncertainty and offset of SRM measurements; ~0.5-1%); (4) uncertainty attributed to common-Pb from inclusions (<1%). According to our estimations on the possible external errors, the propagated errors are in the range of 1.5-2%. Based on these considerations, we applied 2% uncertainty (for 2 sigma errors) on the obtained ages. In the case of the more homogeneous samples (Td-J, Td-H, Td-E, DEMNE-1, FN1) the eruption ages can be approached either by the youngest UNMIX age population or by the weighted mean ages (rejecting the outliers defined by 2σ criteria). They give the same interpretative eruption ages within error except for Td-J, which has a younger interpretative eruption age (based on the youngest age population) than the weighted mean crystallization age. The obtained interpretative eruption ages were compared with the cooling ages derived from the (U-Th)/He data (Table 4). Although the (U-Th)/He ages have higher uncertainty than the U-Pb ages, we observed good agreement between the methods.

Four eruption phases can be distinguished within the studied BVF samples, primarily based on the samples of Tibolddaróc section:

1. The oldest eruption age was determined for the sample Td-J that represents a pyroclastic fall deposit between reworked volcanoclastic deposits, and is stratigraphically the oldest sampled unit of Tibolddaróc section (Fig. 2). The interpreted eruption age of this unit is 15.9±0.3 Ma (Table 4). Márton et al. (2007) suggested that this sample has a normal magnetic polarity and we can compare our proposed age data with the magnetostratigraphic timescale (Gee and Kent 2007). There was a normal polarity subchron between 16.293 and 16.014 Ma (C5Cn.1n) that fits with our interpreted eruption age (Fig. 12). The eruption age could not be younger than 16.014 Ma since this subchron was followed by a relatively long reverse subchron (16.014-15.155 Ma; C5Br) and it probably gives an upper time constraint for the eruption age. The age of this unit indicates that this eruption phase could more likely have been closer to the eruption of the Bogács ignimbrites ("middle rhyolite tuff": 16-17.5 Ma; Márton and Pécskay 1998) and it does not belong to the youngest eruption period of the BVF.
2. The next eruption phase in stratigraphic order of Tibolddaróc section produced the ash-flow tuff of Td-H unit, which yields a 14.8±0.3 Ma eruption age. This is supported by the (U-Th)/He data (14.63±0.61 Ma). The Demjén-Nagyeresztvény (DEMNE-1) ignimbrite, which was previously regarded as one of the youngest volcanic formations in the BVF (K/Ar: 13.84±0.94 Ma; Márton and Pécskay 1998), and the ignimbrite exposed in the Felnémet quarry (FN1) yield a similar age to the Td-H unit: 14.7±0.3 Ma and 14.8±0.3 Ma, respectively. These three samples have relative homogeneous zircon age populations (Tables 1 and 4, Figs. 6

and 7) and their correlation is further confirmed by their remarkably similar zircon and bulk rock trace element geochemistry (Group H zircons, Figs. 8, 10 and 11) and zircon textures (i.e. stumpy zircons, Fig. 5). Thus, they could represent deposits of the same eruption (or part of the same eruption sequence from a given magma storage region). According to Márton and Pécskay (1998) and Márton et al. (2007), both the samples of Demjén-Nagyeresztvény (DEMNE-1) and Felnémet (FN1) quarries show reverse magnetic polarity. There were two shorter reversal periods in magnetic polarity (C5Bn1r and C5ADr) at 15.03-14.88 Ma and 14.80-14.61 Ma, which are in agreement with our interpreted eruption ages (Fig. 12). The eruption age could not be younger than 14.61 Ma as the next reverse polarity subchron was followed by a longer normal polarity subchron (14.61-14.16 Ma; C5ADn).

3. After a short quiescence period represented by a reworked deposit above Td-H unit in the Tibolddaróc section, the volcanic activity resumed at 14.6±0.3 Ma, when repeated eruptions occurred, resulting in a complex pyroclastic sequence. This eruption phase produced the Td-F and Td-E units. Their eruption ages cannot be statistically distinguished from Td-H and the following Td-A unit. We note that compositional characteristics of both the Td-E zircons and Td-F, Td-E bulk rocks resemble those of the younger Td-A ignimbrite (Fig. 11). Therefore, these deposits were likely derived from a separate eruption event, presumably from the Group-2 magma reservoir, which later produced the large volume Td-A ignimbrite.
4. The last major volcanic event, producing the Td-A ignimbrite (Harsány ignimbrite; Lukács et al. 2007; 2009) occurred at 14.1±0.3 Ma, following the reworked deposit above Td-E layer in the Tibolddaróc sequence (implying a shorter lull of volcanism). It can be correlated with the uppermost sample from the drill core of Szv3-1 (Fig. 3), which has the same age as Td-A within error and has similar zircon geochemistry. The interpreted eruption ages are in good agreement with the obtained ID-TIMS result (14.408±0.018 Ma) and the (U-Th)/He ages of the Td-A (14.27±0.59 Ma) and the Szv3-1 samples (14.19±0.60). So far, these are the youngest zircon ages we obtained for the BVF silicic volcanic rocks, which are older than the previously suggested K/Ar ages (13.35±1.01 Ma and 13.65±0.72 Ma for the Harsány ignimbrite; Lukács et al. 2007).

The pyroclastic rocks of Szv3-2 and Mn-2 borehole (Mn2-1 and Mn2-2) samples (Fig. 3) show eruption ages between 14.4-14.7±0.3 Ma which overlap the eruption ages of Td-H and Td-A units, and therefore cannot be correlated either of them based on their zircon ages. Trace element composition of these zircons does not give unambiguous affinity to either main geochemical zircon groups (Group H or A), although they are more similar to Group A.

Implications for the regional geology

The new zircon age data have important implications on the volcanic and tectonic evolution of the Northern Pannonian Basin. The oldest studied pyroclastic unit, Td-J, gives a 15.9±0.3 Ma eruption age, which probably belongs to the "middle rhyolite tuff" and not to the youngest eruption period of the BVF (i.e. "upper rhyolite tuff"). According to the eruption ages obtained from the *in-situ* zircon analyses, at least two eruption phases can be distinguished within the youngest products of the BVF. The older one is represented by the samples belonging to Group-1 (Td-H, DEMNE-1, FN1) and has an eruption age of 14.8±0.3 Ma and we refer this as Demjén Ignimbrite. The location of the eruption source could have been close to the DEMNE-1 locality, where the un-welded to slightly welded ignimbrites have a thickness over 30 m and thus, it could have been southwest-west of

the BVF. Considering the areal distribution (over 300 km^2) and the minimum thickness (15-30 m; Lukács et al. 2007) of the deposit, a conservative estimate for the volume of the volcanic deposits could exceed 10 km^3. It should be noted that a thick ignimbrite with glass shards having strikingly similar trace element signature as DEMNE-1 can be found more than 50 km away (at Tar; Harangi et al. 2005), supporting the evacuation of large volume of tephra during this eruption. The youngest volcanic product containing the Group-2 zircons is the Harsány Ignimbrite (Td-A, Szv3-1) and has an eruption age of 14.1±0.3 Ma. The Td-A unit has a minimum thickness of 30 m at Tibolddaróc and can be correlated with the Szv3-1 deposit having ~ 40 m thickness 5 km away. Furthermore, this unit can be recognized in other boreholes over 10 kms (Lukács et al. 2007; 2010). Thus, it is inferred that this was again a significant eruption, when pyroclastic flows extended over 10's of km and covered a large area (several hundred km^2). The source region is inferred to be close to the Td-A locality, and the estimated volume of the erupted volcanic material could be over 10 km^3. Between these two larger eruption phases, an additional eruption phase (represented by Td-E and Td-F having Group-2 zircon trace element compositional affinity), with typically smaller volumes of erupted products, can be recognized in the stratigraphy of the Tibolddaróc section. This volcanic event could be regarded as a precursor of the voluminous Harsány ignimbrite eruption, tapping the same magma reservoir. Source regions of the two larger eruption phases (Demjén Ignimbrite and Harsány Ignimbrite) seem to have developed at least 10-30 km apart from one another, similarly as the Okataina and Taupo magmatic systems in New Zealand (Charlier et al. 2005; Charlier and Wilson 2010).

The tectonic significance of the new zircon ages is the definition of the limit of two important deformation phases (stress fields) of the Northern Pannonian Basin. The two phases were separated by a 30° CCW block rotation event (Fig. 12). This rotation corresponds to a change in stress field from (E)NE–(W)SW extension to a more strike-slip-dominated stress field with E–W extension and N–S compression (Márton and Fodor 2005, Petrik et al. 2014, 2015). The older stress field marked the classical syn-rift extension in the Pannonian basin, whereas the younger, post-rotational deformation is related to important basin formation in a strike-slip setting south of the BVF (Vatta-Maklár trough, Tari 1988). Tari (1988) and Petrik et al. (2014) demonstrated that the volcanic units studied here were deposited in an actively subsiding graben system. Our new U-Pb zircon age data constrain a maximum age of the start of this deformation of 14.8±0.3 Ma.

Zircon trace element constraints on the magma evolution

While zircon ages provide important constrains on the temporal evolution of silicic magma storage, the internal texture and compositional signatures of the individual grains yield additional information on the nature of the magmas. Trace element composition of zircons is a powerful tool that mirrors the magma evolution and characterizes silicic magmatic systems (Hoskin and Schaltegger 2003; Klemetti et al. 2011; Klemetti and Clynne 2014; Wotzlaw et al. 2013; Chamberlain et al. 2014; Cooper et al. 2014; Storm et al. 2014). Based on the trace element characteristics of the studied BVF zircons, we could distinguish two main groups, denoted as Group-1 (Demjén Ignimbrite) and Group-2 (Harsány Ignimbrite involving the Td-E and Td-F precursor eruption products), which represent distinct magmatic systems. These silicic magma reservoirs evolved partially contemporaneously, but were spatially separated and did not interact with each other, as indicated also by the U-Pb age data (Figs. 6 and 7). In the following, we focus primarily on the magma evolution of these two magmatic systems based on their zircon trace element compositional features.

The evolution of the silicic magmas can be effectively monitored by the Hf content and Th/U and Zr/Hf ratios of the zircons (indicators of the degree of crystal fractionation; Hoskin et al. 2000; Claiborne et al. 2006; 2010) combined with variation in Ti (controlled by crystallization temperature; Watson and Harrison, 2005), and further trace element ratios, which reflect the pre- and co-crystallizing mineral phases (Hoskin et al. 2000). Using these geochemical parameters (Fig. 8 and Online Resource 5), we can conclude that evolution of the magmas fed the two major ignimbrite-forming eruptions was different. The wide range in Hf and Th/U values in the zircons of the Harsány Ignimbrite suggest protracted magma differentiation, whereas these values in Demjén Ignimbrite magma are more restricted. Two subparallel trends can be observed in the Y vs. Th/U diagram, where the Denjén Ignimbrite zircons contain significantly less Y (<2000 ppm; Fig. 10) than those from the Harsány Ignimbrite. In the latter case, Y shows a fan-shaped trend along with U, similar to the Tarawera (Storm et al. 2014) and Mangakino (Cooper et al. 2014) zircons. The Ti-in-zircon thermometer yield low crystallization temperature (670-760 ^{o}C using Ferry and Watson 2007 method with $aTiO_2$=0.7 and $aSiO_2$=1; Fig. 9; Online Resource 3) for both magmas suggesting a relatively cold crystal mush state, close to the solidus temperature (around 680-700 ^{o}C for water-saturated haplogranitic melts; Johannes and Holtz 1996). Zircon saturation temperatures (716-750 ^{o}C; Watson and Harrison 1983; Ryerson and Watson 1987) calculated from the juvenile glasses of Demjén Ignimbrite and Harsány Ignimbrite support this conclusion (Fig. 9; Online Resource 4).

The Eu/Eu* and Yb/Gd ratios (Fig. 8.) suggest pre- and co-crystallization of plagioclase, amphibole and apatite, although in different degrees in the two silicic magma groups. Variation of Nd/Yb and Nd/Gd ratios along Hf and Th/U implies allanite crystallization (Reid et al. 2011) during the latest stage of magma evolution. Indeed, Lukács et al. (2009) described allanite in the Harsány Ignimbrite. The most extreme Eu/Eu* values (< 0.1) in the Group-2 zircons coincide with the highest Hf, U and Th contents suggesting derivation from a highly evolved melt, possibly crystallization in some of the most crystal-rich parts of the magma reservoir. In contrast, a sort of bimodality in Eu/Eu* as well as Ti content can be recognized at the same Hf values in the zircons of the Demjén Ignimbrite samples that could indicate existence of isolated magma batches within the magma reservoir.

The co-existence of a spatially non-connected magma systems with distinct silicic magma types is corroborated by further trace element signatures. In the zircons of the Demjén Ignimbrite samples, Nb and Ta are depleted (up to 5 and 1.5 ppm, respectively) and have high Hf/Nb ratio (>2000), whereas the zircons of the Harsány Ignimbrite samples have typically low Hf/Nb ratio (mostly less than 2000) and are enriched in Nb and Ta (mostly above 5 and 1 ppm, respectively). The HFSE content in zircons could reflect the composition of their parental magmas and is higher mostly in the alkaline granitic rocks (Nardi et al. 2013). In general, such zircons have also higher Nb/Ta ratios and deeper negative Eu-anomaly, which can be observed in the zircons of the Harsány Ignimbrite samples (Online Resource 5). This could suggest that the zircons of the two ignimbrite units were formed from different types of silicic magmas generated from distinct source regions. The contrasting behaviour of HFSE in the BVF zircons can be observed also in other silicic volcanic systems. Zircons from the Bishop tuff show Nb enrichment along with increasing Hf (Chamberlain et al. 2014), whereas zircons from the Mangakino ignimbrites, Taupo zone (Cooper et al. 2014) have dominantly low Nb concentration, which does not vary with increasing Hf. The reason of this dichotomy is still unresolved and warrants further research.

The nature and lifetime of the silicic magma reservoirs

The lifetime of silicic magma storage can be deduced from the zircon crystallization ages of single samples. The silicic magma reservoirs of the BVF could have persisted over 300-700 kyr. Zircons evolved mostly in a relatively cold crystal mush environment as indicated by the Ti in zircon thermometry and the relatively low Zr/Hf and Th/U ratios. The zircons of the Demjén Ignimbrite samples indicate existence of isolated magma batches within the magma reservoir. Distinct magma batches were suggested also for the Td-A magma based on the bimodal pumice composition (Lukács et al. 2009), but this cannot be recognized unambiguously in the zircon chemistry. Nevertheless, the studied BVF ignimbrites are crystal-poor products and therefore derive from melt-dominated lenses. Thus, evolved melts from the magma differentiation zones have assembled into a common melt-dominated lens, presumably just before the eruption, as discussed for a number of silicic volcanic units worldwide (Shane et al. 2008; Cooper et al. 2012; Ellis and Wolff 2012; Bégué et al. 2014; Wotzlaw et al. 2014; 2015). This resulted in evacuation of crystal-poor magmas, but with a zircon crystal cargo preserving the heterogeneous, long-lived compositional character of the magma storage.

It is now commonly assumed that silicic magmatic reservoirs can grow incrementally by repeated recharge from below (see Hildreth 2004; Lipman 2007 and Glazner et al. 2008 for reviews). The large range of crystallization ages and the heterogeneous trace element character of the zircon cargo in single samples suggest a magma storage in a partly mushy state over prolonged period (Koyaguchi and Kaneko 1999; Brown and Fletcher 1999; Bachmann and Bergantz 2004; Miller et al. 2007; Huber et al. 2010; Gelman et al. 2013; Wotzlaw et al. 2013). This condition could enable an effective recycling of the zircon antecryst population before the eruption. We do not exclude that intermittent pulses of new magmas could arrive into the magma storage where they are solidified within a short (<50 ka) time range (Sparks et al., 1990; Schmitt et al., 2010; Simon et al., 2014). Such magma batches could be partially reactivated upon the arrival of a new magma batch. Zircon grains with up to 700 ka intra-crystal age differences could reflect such evolution. In this context, we consider that the warmest parts of the magma reservoir can remain in a mushy state for several 100's ka, even up to 700 ka, similar to silicic plutons (Walker et al. 2007; Schaltegger et al. 2009; Schoene et al. 2012; Lipman and Bachmann 2015), while peripheral zones could enter sub-solidus conditions. When the solidified and mushy parts are reactivated, zircons can be recycled in the interstitial melt and continue growing. This mechanism is supported by the commonly observed resorption zones within the studied zircons (see Online Resource 1). These zircons can be regarded as antecrysts, since they belong to the evolution of the same magma storage, as shown both by their U/Pb dates (within the time range of the population) and their trace element compositions (consistent with the population). Intermittent mixing could partly or wholly re-homogenize the mushy system and could preserve the zircons formed at different stages and times in the evolved melt pockets. Such large-scale mixing in the crystal mush was suggested based on the occurrence of antecrystic crystal cargo in the crystal-rich volcanic products of the Bogács unit by Czuppon et al. (2012) also in the BVF.

Although we conclude that most of the studied zircons could be antecrysts, we have to note that the analysed zircons were separated from the 63-125 μm sized fraction and we analysed only grains, which had a certain width (larger than ca. 60 μm). There are also elongated narrow zircons in some samples, which notably gave the youngest ages when reliable ages could be determined (e.g., Td-A, Fig. 4). Thus, these zircons might have crystallized not long before the eruption, possibly from the silicic melt lens and therefore they can be regarded as phenocrysts.

For such long upper crustal magma storage durations, sustained heat-flux via repeated arrival of mantle-derived basaltic magma into the crustal column is necessary (Memeti et al. 2010; Gelman et al. 2013). The heat-flux in the Pannonian Basin is still anomalously high (100-120 mW/m^2; Lenkey et al. 2002; Horváth et al. 2015) and is characterized by steep geothermal gradient consistent with thin crust (< 30 km) and lithosphere (< 80 km). During the Middle Miocene the heat-flux could have been even higher when the initially thick lithosphere stretched to more than half of the original thickness (Horváth 1993; Tari et al. 1999). The thinned continental crust underwent a major thermal maturation providing a suitable situation for crustal magmatism and the existence of long lasting magma reservoirs. A similar significant tectonomagmatic event, although in a different plate tectonic environment, occurred in the southwestern North America during the Mid-Tertiary (Lipman et al. 1971; Lipman and Glazner 1991) and was dubbed an "ignimbrite flare-up" (Coney 1978). This concept was introduced also to the silicic magmatism of the Altiplano-Puna, Central Andes by De Silva (1989). We suggest that such an ignimbrite flare-up event with strong thermomechanical influence on the crust could have occurred also during the Middle Miocene major extensional phase of the Pannonian Basin.

Conclusions

This study reports an attempt to better constrain the ages of the youngest period of silicic volcanism of the northern Pannonian Basin using U/Pb and (U-Th)/He geochronology on zircons. Beyond the obtained TIMS data on single crystals, the individual in-situ ages determined by LA-ICP-MS technique help to identify the pre-eruption residence time of the silicic magma reservoirs related to major ignimbrite-forming eruptions. The youngest age populations isolated from the spot ages coincide well with the zircon (U-Th)/He data as well as ID-TIMS result and record the closest age of eruption. Magnetic polarity data also support and bracket the interpreted eruption ages obtained from the LA-ICP-MS data set. Our results show that zircon U-Pb geochronology coupled with zircon geochemistry provides a powerful tool to correlate volcanic deposits of Middle Miocene (Badenian) age within a selectively eroded area and likely could help in correlation with far-away ash layers or cryptotephras as well. Correlating the eruption events with the regional magnetic polarity periods and the obtained palaeomagnetic declination data from the BVF, we constrain the upper temporal boundary (15 Ma) of the youngest CCW rotation in the northern part of the Pannonian Basin and at the same time, the beginning of a new deformation phase, a strike-slip-dominated one of the Vatta-Maklár trough.

Based on our new geochronological data, we can recognize waxing and waning phases of magmatic evolution during the younger stage of the Middle Miocene ignimbrite flare-up period in the Pannonian Basin. Two voluminous (>10 km^3) and one smaller eruption phases were distinguished within the youngest (14-15 Ma) episode of this volcanism. Following the large volcanic eruptions, due to potential "freezing" of the left-over mush by the rapid syn-eruptive decompression, new magma storage started to develop, accumulating silicic magma batches derived from slightly different sources. This is reflected both by the compositional differences of zircons and the distinct compositions of the juvenile materials. The individual silicic magma reservoirs could exist mostly in a mushy state over 300-700 kyr, sustained by the high heat-flow and the steep crustal geothermal gradient during the main lithospheric stretching phase of the Pannonian Basin. During the eruption stages evacuation of mostly crystal-poor melts occurred. We demonstrate here that even crystal-poor rhyolitic ignimbrites can contain zircons with wide age range possibly covering most of the lifetime of the magma reservoir.

Acknowledgements

The study was supported by the Hungarian National Research, Development and Innovation (NKFI) Fund OKTA K81530 and OTKA PD112584. Réka Lukács was supported by the Bolyai János Research Fellowship and the Campus Hungary Fellowship (B2/4R/12728). Constructive comments by two anonymous reviewers and by Othmar Müntener as the Editor helped to improve the original version of the manuscript.

References

Annen C, Blundy JD, Leuthold J, Sparks RSJ (2015) Construction and evolution of igneous bodies: Towards an integrated perspective of crustal magmatism. Lithos 230:206-221

Aydar E, Schmitt AK, Çubukçu HE, Akin L, Ersoy O, Sen E, Duncan RA, Atici G (2012) Correlation of ignimbrites in the central Anatolian volcanic province using zircon and plagioclase ages and zircon compositions. Journal of Volcanology and Geothermal Research 213–214:83-97

Bachmann O, Bergantz G (2008) The Magma Reservoirs That Feed Supereruptions. Elements 4(1):17-21

Bachmann O, Bergantz GW (2003) Rejuvenation of the Fish Canyon magma body: A window into the evolution of large-volume silicic magma systems. Geology 31(9):789-792

Bachmann O, Bergantz GW (2004) On the Origin of Crystal-poor Rhyolites: Extracted from Batholithic Crystal Mushes. Journal of Petrology 45(8):1565-1582

Bachmann O, Charlier BLA, Lowenstern JB (2007) Zircon crystallization and recycling in the magma chamber of the rhyolitic Kos Plateau Tuff (Aegean arc). Geology 35(1):73-76

Bachmann O, Deering C, Ruprecht J, Huber C, Skopelitis A, Schnyder C (2012) Evolution of silicic magmas in the Kos-Nisyros volcanic center, Greece: a petrological cycle associated with caldera collapse. Contrib Mineral Petrol 163(1):151-166

Bachmann O, Dungan MA, Lipman PW (2002) The Fish Canyon Magma Body, San Juan Volcanic Field, Colorado: Rejuvenation and Eruption of an Upper-Crustal Batholith. Journal of Petrology 43(8):1469-1503

Bachmann O, Oberli F, Dungan MA, Meier M, Mundil R, Fischer H (2007) 40Ar/39Ar and U–Pb dating of the Fish Canyon magmatic system, San Juan Volcanic field, Colorado: Evidence for an extended crystallization history. Chemical Geology 236(1–2):134-166

Bachmann O, Schoene B, Schnyder C, Spikings R (2010) The 40Ar/39Ar and U/Pb dating of young rhyolites in the Kos-Nisyros volcanic complex, Eastern Aegean Arc, Greece: Age discordance due to excess 40Ar in biotite. Geochemistry, Geophysics, Geosystems 11(8):Q0AA08

Bacon CR, Lowenstern JB (2005) Late Pleistocene granodiorite source for recycled zircon and phenocrysts in rhyodacite lava at Crater Lake, Oregon. Earth and Planetary Science Letters 233(3–4):277-293

Bégué F, Deering CD, Gravley DM, Kennedy BM, Chambefort I, Gualda GAR, Bachmann O (2014) Extraction, Storage and Eruption of Multiple Isolated Magma Batches in the Paired Mamaku and Ohakuri Eruption, Taupo Volcanic Zone, New Zealand. Journal of Petrology 55(8):1653-1684

Black LP, Kamo SL, Allen CM, Davis DW, Aleinikoff JN, Valley JW, Mundil R, Campbell IH, Korsch RJ, Williams IS, Foudoulis C (2004) Improved 206Pb/238U microprobe geochronology by the monitoring

of a trace-element-related matrix effect; SHRIMP, ID–TIMS, ELA–ICP–MS and oxygen isotope documentation for a series of zircon standards. Chemical Geology 205(1–2):115-140

Brown SJA, Fletcher IR (1999) SHRIMP U-Pb dating of the preeruption growth history of zircons from the 340 ka Whakamaru Ignimbrite, New Zealand: Evidence for >250 k.y. magma residence times. Geology 27(11):1035-1038

Chamberlain KJ, Wilson CJN, Wooden JL, Charlier BLA, Ireland TR (2014) New Perspectives on the Bishop Tuff from Zircon Textures, Ages and Trace Elements. Journal of Petrology 55(2):395-426

Charlier BLA, Wilson CJN (2010) Chronology and Evolution of Caldera-forming and Post-caldera Magma Systems at Okataina Volcano, New Zealand from Zircon U–Th Model-age Spectra. Journal of Petrology 51(5):1121-1141

Charlier BLA, Wilson CJN, Lowenstern JB, Blake S, Van Calsteren PW, Davidson JP (2005) Magma Generation at a Large, Hyperactive Silicic Volcano (Taupo, New Zealand) Revealed by U–Th and U–Pb Systematics in Zircons. Journal of Petrology 46(1):3-32

Claiborne LL, Miller CF, Walker BA, Wooden JL, Mazdab FK, Bea F (2006) Tracking magmatic processes through Zr/Hf ratios in rocks and Hf and Ti zoning in zircons: An example from the Spirit Mountain batholith, Nevada. Mineralogical Magazine 70(5):517-543

Claiborne LL, Miller CF, Flanagan DM, Clynne MA, Wooden JL (2010) Zircon reveals protracted magma storage and recycling beneath Mount St. Helens. Geology 38(11):1011-1014

Compston W, Williams IS, Meyer C (1984) U-Pb geochronology of zircons from lunar breccia 73217 using a sensitive high mass-resolution ion microprobe. Journal of Geophysical Research: Solid Earth 89(S02):B525-B534

Coney PJ (1978) Mesozoic–Cenozoic Cordilleran plate tectonics. In: Smith RB, Eaton GP (eds) Cenozoic tectonics and regional geophysics of the western Cordillera. Geol Soc Am Mem 152:33-50

Cooper G, Wilson CN, Charlier BA, Wooden J, Ireland T (2014) Temporal evolution and compositional signatures of two supervolcanic systems recorded in zircons from Mangakino volcanic centre, New Zealand. Contrib Mineral Petrol 167(6):1-23

Cooper GF, Wilson CJN, Millet M-A, Baker JA, Smith EGC (2012) Systematic tapping of independent magma chambers during the 1 Ma Kidnappers supereruption. Earth and Planetary Science Letters 313–314:23-33

Cooper KM, Kent AJR (2014) Rapid remobilization of magmatic crystals kept in cold storage. Nature 506:480-483

Costa F (2008) Residence Times of Silicic Magmas Associated with Calderas. In: Joachim Gottsmann, Joan Marti (eds) Developments in Volcanology, Volume 10, Elsevier, pp 1-55

Czuppon G, Lukács R, Harangi S, Mason PRD, Ntaflos T (2012) Mixing of crystal mushes and melts in the genesis of the Bogács Ignimbrite suite, northern Hungary: An integrated geochemical investigation of mineral phases and glasses. Lithos 148:71-85

Danišík M, Shane P, Schmitt AK, Hogg A, Santos GM, Storm S, Evans NJ, Keith Fifield L, Lindsay JM (2012) Re-anchoring the late Pleistocene tephrochronology of New Zealand based on concordant radiocarbon ages and combined 238U/230Th disequilibrium and (U–Th)/He zircon ages. Earth and Planetary Science Letters 349–350:240-250

Danišík M, Fodor L, Dunkl I, Gerdes A, Csizmeg J, Hámor-Vidó M, Evans NJ (2015) A multi-system geochronology in the Ad-3 borehole, Pannonian Basin (Hungary) with implications for dating volcanic rocks by low-temperature thermochronology and for interpretation of (U-Th)/He data. Terra Nova 27:258–269

Deering CD, Bachmann O, Vogel TA (2011) The Ammonia Tanks Tuff: Erupting a melt-rich rhyolite cap and its remobilized crystal cumulate. Earth and Planetary Science Letters 310(3–4):518-525

de Silva SL (1989) Altiplano-Puna volcanic complex of the central Andes. Geology 17:1102–1106

Dunkl I, Árkai P, Balogh K, Csontos L, Nagy G (1994) Modelling the thermal history using fission track data - Exhumation of Bükk Mountains, Inner Western Carpathians (in Hungarian with English abstract). Földtani Közlöny 124:1-24

Ellis BS, Wolff JA (2012) Complex storage of rhyolite in the central Snake River Plain. Journal of Volcanology and Geothermal Research 211–212:1-11

Evans NJ, Byrne JP, Keegan JT, Dotter LE (2005) Determination of Uranium and Thorium in zircon, apatite, and fluorite: Application to laser (U-Th)/He thermochronology. Journal of Analytical Chemistry 60(12):1159-1165

Farley KA (2002) (U-Th)/He Dating: Techniques, Calibrations, and Applications. Reviews in Mineralogy and Geochemistry 47(1):819-844

Farley KA, Wolf RA, Silver LT (1996) The effects of long alpha-stopping distances on (U-Th)/He ages. Geochimica et Cosmochimica Acta 60(21):4223-4229

Ferry JM, Watson EB (2007) New thermodynamic models and revised calibrations for the Ti-in-zircon and Zr-in-rutile thermometers. Contrib Mineral Petrol 154(4):429-437

Frazer RE, Coleman DS, Mills RD (2014) Zircon U-Pb geochronology of the Mount Givens Granodiorite: Implications for the genesis of large volumes of eruptible magma. Journal of Geophysical Research: Solid Earth 119(4):2013JB010716

Gebauer S, Schmitt A, Pappalardo L, Stockli D, Lovera O (2014) Crystallization and eruption ages of Breccia Museo (Campi Flegrei caldera, Italy) plutonic clasts and their relation to the Campanian ignimbrite. Contrib Mineral Petrol 167(1):1-18

Gee JS, Kent DV (2007) 5.12 - Source of Oceanic Magnetic Anomalies and the Geomagnetic Polarity Timescale. In: Schubert G (ed) Treatise on Geophysics, vol. Elsevier, Amsterdam, pp 455-507

Gehrels GE, Valencia VA, Ruiz J (2008) Enhanced precision, accuracy, efficiency, and spatial resolution of U-Pb ages by laser ablation–multicollector–inductively coupled plasma–mass spectrometry. Geochemistry, Geophysics, Geosystems 9(3):Q03017

Gelman SE, Gutiérrez FJ, Bachmann O (2013) On the longevity of large upper crustal silicic magma reservoirs. Geology 41:759-762

Ghiorso M, Gualda GR (2013) A method for estimating the activity of titania in magmatic liquids from the compositions of coexisting rhombohedral and cubic iron–titanium oxides. Contrib Mineral Petrol 165(1):73-81

Glazner AF, Bartley JM, Coleman DS, Gray W, Taylor RZ (2004) Are plutons assembled over millions of years by amalgamation from small magma chambers? GSA Today 14:4-11

Glazner AF, Coleman DS, Bartley JM (2008) The tenuous connection between high-silica rhyolites and

granodiorite plutons. Geology 36(2):183-186

Glazner, A., Coleman, D. & Mills, R. (2015). The Volcanic-Plutonic Connection. Springer Berlin Heidelberg, 1-22.

Guenthner WR, Reiners PW, Ketcham RA, Nasdala L, Giester G (2013) Helium diffusion in natural zircon: Radiation damage, anisotropy, and the interpretation of zircon (U-Th)/He thermochronology. American Journal of Science 313(3):145-198

Guillong M, Meier DL, Allan MM, Heinrich CA, Yardley BWD (2008) SILLS: A MATLAB-based program for the reduction of laser ablation ICP-MS data of homogeneous materials and inclusions. Mineralogical Association of Canada Short Course 40:328-333

Guillong M, von Quadt A, Sakata S, Peytcheva I, Bachmann O (2014) LA-ICP-MS Pb-U dating of young zircons from the Kos-Nisyros volcanic centre, SE Aegean arc. Journal of Analytical Atomic Spectrometry 29(6):963-970

Hámor G, Pogácsás G, Jámbor Á (2001) Paleogeographic/structural evolutionary stages and the related volcanism of the Carpathian-Pannonian Region. Acta Geologica Hungarica 44:193-222

Harangi S, Lenkey L (2007) Genesis of the Neogene to Quaternary volcanism in the Carpathian-Pannonian region: Role of subduction, extension, and mantle plume. Geological Society of America Special Papers 418:67-92

Harangi S, Lukács R (2009) On the age of the Harsány ignimbrite, Bükkalja volcanic field, Northern Hungary – a discussion. Central European Geology 52(1):43-50

Harangi S, Lukács R, Schmitt AK, Dunkl I, Molnár K, Kiss B, Seghedi I, Novothny Á, Molnár M (2015) Constraints on the timing of Quaternary volcanism and duration of magma residence at Ciomadul volcano, east–central Europe, from combined U–Th/He and U–Th zircon geochronology. Journal of Volcanology and Geothermal Research 301:66-80

Harangi S, Mason PRD, Lukács R (2005) Correlation and petrogenesis of silicic pyroclastic rocks in the Northern Pannonian Basin, Eastern-Central Europe: In situ trace element data of glass shards and mineral chemical constraints. Journal of Volcanology and Geothermal Research 143(4):237-257

Hildreth W (2004) Volcanological perspectives on Long Valley, Mammoth Mountain, and Mono Craters: several contiguous but discrete systems. Journal of Volcanology and Geothermal Research 136(3–4):169-198

Hildreth W, Wilson CJN (2007) Compositional Zoning of the Bishop Tuff. Journal of Petrology 48(5):951-999

Horváth F (1993) Towards a mechanical model for the formation of the Pannonian basin. Tectonophysics 226(1–4):333-357

Horváth F, Bada G, Szafián P, Tari G, Ádám A, Cloetingh S (2006) Formation and deformation of the Pannonian Basin: constraints from observational data. Geological Society, London, Memoirs 32(1):191-206

Horváth F, Musitz B, Balázs A, Végh A, Uhrin A, Nádor A, Koroknai B, Pap N, Tóth T, Wórum G (2015) Evolution of the Pannonian basin and its geothermal resources. Geothermics 53:328-352

Horváth F, Royden LH (1981) Mechanism for formation of the intra-Carpathian basins: A review. Earth. Evol. Sci. 1:307-316

Hoskin PWO, Kinny PD, Wyborn D, Chappell BW (2000) Identifying Accessory Mineral Saturation during Differentiation in Granitoid Magmas: an Integrated Approach. Journal of Petrology 41(9):1365-1396

Hoskin PWO, Schaltegger U. (2003) The Composition of Zircon and Igneous and Metamorphic Petrogenesis:

Reviews in Mineralogy and Geochemistry 53(1):27-62.

Huber C, Bachmann O, Dufek J (2010) The limitations of melting on the reactivation of silicic mushes. Journal of Volcanology and Geothermal Research 195(2–4):97-105

Huppert HE, Sparks RSJ (1988) The Generation of Granitic Magmas by Intrusion of Basalt into Continental Crust. Journal of Petrology 29(3):599-624

Hurai V, Danišík M, Huraiová M, Paquette J-L, Ádám A (2013) Combined U/Pb and (U–Th)/He geochronometry of basalt maars in Western Carpathians: implications for age of intraplate volcanism and origin of zircon metasomatism. Contrib Mineral Petrol 166(4):1235-1251

Iwano H, Orihashi Y, Hirata T, Ogasawara M, Danhara T, Horie K, Hasebe N, Sueoka S, Tamura A, Hayasaka Y, Katsube A, Ito H, Tani K, Kimura J-I, Chang Q, Kouchi Y, Haruta Y, Yamamoto K (2013) An inter-laboratory evaluation of OD-3 zircon for use as a secondary U–Pb dating standard. Island Arc 22(3):382-394

Jackson SE, Pearson NJ, Griffin WL, Belousova EA (2004) The application of laser ablation-inductively coupled plasma-mass spectrometry to in situ U–Pb zircon geochronology. Chemical Geology 211(1–2):47-69

Jaffey AH, Flynn KF, Glendenin LE, Bentley WC, Essling AM (1971) Precision Measurement of Half-Lives and Specific Activities of 235U and 238U. Physical Review C 4(5):1889-1906

Johannes W, Holtz F (1996) Petrogenesis and experimental petrology of granitic rocks. Springer-Verlag, Berlin:335 p.

Klemetti EW, Clynne MA (2014) Localized rejuvenation of a crystal mush recorded in zircon temporal and compositional variation at the Lassen Volcanic Center, northern California. PLoS ONE 9(12):e113157

Klemetti EW, Deering CD, Cooper KM, Roeske SM (2011): Magmatic perturbations in the Okataina Volcanic Complex, New Zealand at thousand-year timescales recorded in single zircon crystals. Earth and Planetary Science Letters 305(1):185-194

Košler J, Sylvester PJ (2003) Present Trends and the Future of Zircon in Geochronology: Laser Ablation ICPMS. Reviews in Mineralogy and Geochemistry 53(1):243-275

Koyaguchi T, Kaneko K (1999) A two-stage thermal evolution model of magmas in continental crust. Journal of Petrology 40:241-254

Lee JKW, Williams IS, Ellis DJ (1997) Pb, U and Th diffusion in natural zircon. Nature 390:159-162

Lenkey L, Dövényi P, Horváth F, Cloetingh S (2002) Geothermics of the Pannonian Basin and its bearing on the neotectonics. EGU Stephan Mueller Special Publications Series, 3:29-40

Less Gy, Kovács S, Pelikán P, Pentelényi L, Sásdi L (2005a) Geology of the Bükk Mountains. Magyar Állami Földtani Intézet, Budapest:284 p.

Less Gy, Gulácsi Z, Kovács S, Pelikán P, Pentelényi L, Rezessy A, Sásdi L (2005b) Geological map of the Bükk Mountains 1: 50 000. Magyar Állami Földtani Intézet, Budapest

Lipman PW (2007) Incremental assembly and prolonged consolidation of Cordilleran magma chambers: Evidence from the Southern Rocky Mountain volcanic field. Geosphere 3(1):42-70

Lipman PW, Glazner AF (1991) Introduction to Middle Tertiary Cordilleran volcanism: magma sources and relations to regional tectonics. J Geophys Res 96:13193–13199

Lipman PW, Bachmann O (2015) Ignimbrites to batholiths: Integrating perspectives from geological, geophysical, and geochronological data. Geosphere 11(3):705–743

Lipman PW, Prostka HJ, Christiansen RL. (1971): Evolving subduction zones in the Western United States, as interpreted from igneous rocks. Science 174:821-825.

Ludwig KR (2012) Isoplot, A Geochronological Toolkit for Microsoft Excel. Berkeley Geochronology Center, Special Publication 5:75 p.

Lukács R, Harangi S, Mason PRD, Ntaflos T (2009) Bimodal pumice populations in the 13.5 Ma Harsány ignimbrite, Bükkalja Volcanic Field, Northern Hungary: syn-eruptive mingling of distinct rhyolitic magma batches? Central European Geology 52(1):51-72

Lukács R, Harangi S, Ntaflos T, Koller F, Pécskay Z (2007) A Bükkalján megjelenő felső riolittufaszint vizsgálati eredményei: a harsányi ignimbrit egység. Földtani Közlöny 137(4):487-514.

Lukács R, Harangi S, Ntaflos T, Mason PRD (2005) Silicate melt inclusions in the phenocrysts of the Szomolya Ignimbrite, Bükkalja Volcanic Field (Northern Hungary): Implications for magma chamber processes. Chemical Geology 223(1–3):46-67

Lukács R, Harangi S, Radócz G, Kádár M, Pécskay Z, Ntaflos T (2010) A Nyékládháza-1, Miskolc-7 és Miskolc-8 sz. fúrások miocén vulkáni kőzetei és párhuzamosításuk a Bükkalja vulkáni képződményeivel. Földtani Közlöny 140(1):31-48

Marillo-Sialer E, Woodhead J, Hergt J, Greig A, Guillong M, Gleadow A, Evans N, Paton C (2014) The zircon 'matrix effect': evidence for an ablation rate control on the accuracy of U-Pb age determinations by LA-ICP-MS. Journal of Analytical Atomic Spectrometry 29(6):981-989

Márton E, Fodor L (1995) Combination of palaeomagnetic and stress data—a case study from North Hungary. Tectonophysics 242(1–2):99-114

Márton E, Pécskay Z (1998) Complex evaluation of paleomagnetic and K/Ar isotope data of the Miocene ignimbritic volcanics in the Bükk Foreland, Hungary. Acta Geologica Hungarica 41:467-476.

Márton E, Zelenka T, Márton P (2007) Paleomagnetic correlation of Miocene pyroclastics of the Bükk Mts. and their forelands. Central European Geology 50(1):47-57

Mattinson JM (2005) Zircon U–Pb chemical abrasion ("CA-TIMS") method: Combined annealing and multi-step partial dissolution analysis for improved precision and accuracy of zircon ages. Chemical Geology 220(1–2):47-66

Memeti V, Paterson S, Matzel J, Mundil R, Okaya D (2010) Magmatic lobes as "snapshots" of magma chamber growth and evolution in large, composite batholiths: An example from the Tuolumne intrusion, Sierra Nevada, California. Geological Society of America Bulletin 122(11-12):1912-1931

Miller JS, Matzel JEP, Miller CF, Burgess SD, Miller RB (2007) Zircon growth and recycling during the assembly of large, composite arc plutons. Journal of Volcanology and Geothermal Research 167(1–4):282-299

Mills RD (2012) Re-evaluating pluton/volcano connections and igneous textures in light of incremental magma emplacement. PhD Thesis Chapel Hill. North Carolina, University of North Carolina:99 p.

Nardi LVS, Formoso MLL, Müller IF, Fontana E, Jarvis K, Lamarão C (2013) Zircon/rock partition coefficients of REEs, Y, Th, U, Nb, and Ta in granitic rocks: Uses for provenance and mineral exploration purposes. Chemical Geology 335:1-7

Nemchin AA, Horstwood MSA, Whitehouse MJ (2013) High-Spatial-Resolution Geochronology. Elements 9(1):31-37

Paquette J-L, Le Pennec J-L (2012) 3.8 Ga zircons sampled by Neogene ignimbrite eruptions in Central Anatolia.

Geology 40(3):239-242

Paton C, Hellstrom J, Paul B, Woodhead J, Hergt J (2011) Iolite: Freeware for the visualisation and processing of mass spectrometric data. Journal of Analytical Atomic Spectrometry 26(12):2508-2518

Paton C, Woodhead JD, Hellstrom JC, Hergt JM, Greig A, Maas R (2010) Improved laser ablation U-Pb zircon geochronology through robust downhole fractionation correction. Geochemistry, Geophysics, Geosystems 11(3):Q0AA06

Pécskay Z, Lexa J, Szakács A, Seghedi I, Balogh K, Konecny V, Zelenka T, Kovac M, Póka T, Fülöp A, Márton E, Panaiotu C, Cvetkovic V (2006) Geochronology of Neogene magmatism in the Carpathian arc and intra-Carpathian area. Geologica Carpathica 57:511-530

Petrik A, Beke B, Fodor L (2014) Combined analysis of faults and deformation bands reveals the Cenozoic structural evolution of the southern Bükk foreland (Hungary). Tectonophysics 633:43-62

Petrik A, Beke B, Fodor L, Lukács R (2015) Cenozoic structural evolution of the southwestern Bükk Mts. and the southern part of the Darnó Deformation Belt (NE Hungary). Geologica Carpathica in press

Petrus JA, Kamber BS (2012) VizualAge: A Novel Approach to Laser Ablation ICP-MS U-Pb Geochronology Data Reduction. Geostandards and Geoanalytical Research 36(3):247-270

Reid M, Vazquez J, Schmitt A (2011) Zircon-scale insights into the history of a Supervolcano, Bishop Tuff, Long Valley, California, with implications for the Ti-in-zircon geothermometer. Contrib Mineral Petrol 161(2):293-311

Reid MR, Coath CD (2000) In situ U-Pb ages of zircons from the Bishop Tuff: No evidence for long crystal residence times. Geology 28(5):443-446

Reiners PW (2005) Zircon (U–Th)/He thermochronometry. Mineral Soc. Am. Rev. Mineral Geochem 58:151-179

Reiners PW, Farley KA, Hickes HJ (2002) He diffusion and (U–Th)/He thermochronometry of zircon: initial results from Fish Canyon Tuff and Gold Butte. Tectonophysics 349(1–4):297-308

Reiners PW, Spell TL, Nicolescu S, Zanetti KA (2004) Zircon (U-Th)/He thermochronometry: He diffusion and comparisons with 40Ar/39Ar dating. Geochimica et Cosmochimica Acta 68(8):1857-1887

Ryerson FJ, Watson EB (1987) Rutile saturation in magmas: implications for Ti-Nb-Ta depletion in orogenic rock series. Earth Planetary Science Letters 86:225-239.

Sambridge MS, Compston W (1994) Mixture modeling of multi-component data sets with application to ion-probe zircon ages. Earth and Planetary Science Letters 128(3–4):373-390

Schaltegger U, Brack P, Ovtcharova M, Peytcheva I, Schoene B, Stracke A, Marocchi M, Bargossi GM (2009) Zircon and titanite recording 1.5 million years of magma accretion, crystallization and initial cooling in a composite pluton (southern Adamello batholith, northern Italy). Earth and Planetary Science Letters 286(1–2):208-218

Schmitt A, Danišík M, Evans N, Siebel W, Kiemele E, Aydin F, Harvey J (2011) Acigöl rhyolite field, Central Anatolia (part 1): high-resolution dating of eruption episodes and zircon growth rates. Contrib Mineral Petrol 162(6):1215-1231

Schmitt AK, Stockli DF, Hausback BP (2006) Eruption and magma crystallization ages of Las Tres Vírgenes (Baja California) constrained by combined 230Th/238U and (U–Th)/He dating of zircon. Journal of Volcanology and Geothermal Research 158(3–4):281-295

Schmitt AK, Stockli DF, Lindsay JM, Robertson R, Lovera OM, Kislitsyn R (2010) Episodic growth and

homogenization of plutonic roots in arc volcanoes from combined U–Th and (U–Th)/He zircon dating. Earth and Planetary Science Letters 295(1–2):91-103

Schoene B, Schaltegger U, Brack P, Latkoczy C, Stracke A, Günther D (2012) Rates of magma differentiation and emplacement in a ballooning pluton recorded by U–Pb TIMS-TEA, Adamello batholith, Italy. Earth and Planetary Science Letters 355–356:162-173

Shane P, Nairn IA, Smith VC (2005) Magma mingling in the ~50 ka Rotoiti eruption from Okataina Volcanic Centre: implications for geochemical diversity and chronology of large volume rhyolites. Journal of Volcanology and Geothermal Research 139(3–4):295-313

Shane P, Martin SB, Smith VC, Beggs KF, Darragh MB, Cole JW, Nairn IA (2007) Multiple rhyolite magmas and basalt injection in the 17.7 ka Rerewhakaaitu eruption episode from Tarawera volcanic complex, New Zealand. Journal of Volcanology and Geothermal Research 164(1–2):1-26

Shane P, Nairn IA, Smith VC, Darragh M, Beggs K, Cole JW (2008): Silicic recharge of multiple rhyolite magmas by basaltic intrusion during the 22.6 ka Okareka Eruption Episode, New Zealand. Lithos 103(3):527-549.

Simon J, Weis D, DePaolo D, Renne P, Mundil R, Schmitt A (2014) Assimilation of preexisting Pleistocene intrusions at Long Valley by periodic magma recharge accelerates rhyolite generation: rethinking the remelting model. Contrib Mineral Petrol 167(1):1-34

Simon JI, Renne PR, Mundil R (2008) Implications of pre-eruptive magmatic histories of zircons for U–Pb geochronology of silicic extrusions. Earth and Planetary Science Letters 266(1–2):182-194

Sláma J, Košler J, Condon DJ, Crowley JL, Gerdes A, Hanchar JM, Horstwood MSA, Morris GA, Nasdala L, Norberg N, Schaltegger U, Schoene B, Tubrett MN, Whitehouse MJ (2008) Plešovice zircon — A new natural reference material for U–Pb and Hf isotopic microanalysis. Chemical Geology 249(1–2):1-35

Smith VC, Shane P, Nairn IA (2004) Reactivation of a rhyolitic magma body by new rhyolitic intrusion before the 15.8 ka Rotorua eruptive episode: implications for magma storage in the Okataina Volcanic Centre, New Zealand. Journal of the Geological Society 161(5):757-772

Sparks RSJ, Huppert HE, Wilson CJN (1990) Comment on "Evidence for long residence times of rhyolitic magma in the Long Valley magmatic system: the isotopic record in precaldera lavas of Glass Mountain" by A.N. Halliday, G.A. Mahood, P. Holden, J.M. Metz, T.J. Dempster and J.P. Davidson. Earth and Planetary Science Letters 99(4):387-389

Storm S, Schmitt A, Shane P, Lindsay J (2014) Zircon trace element chemistry at sub-micrometer resolution for Tarawera volcano, New Zealand, and implications for rhyolite magma evolution. Contributions to Mineralogy and Petrology 167:1000

Sun SS, McDonough WF (1989) Chemical and isotopic systematics of oceanic basalts: implications for mantle composition and processes. In: Saunders AD, Norry MJ (Eds.), Magmatism in the oceanic basins, Geol. Soc. Spec. Publ. No.42:313-345

Szabó C, Harangi S, Csontos L (1992) Review of Neogene and Quaternary volcanism of the Carpathian-Pannonian region. Tectonophysics 208(1–3):243-256

Szakács A, Zelenka T, Márton E, Pécskay Z, Póka T, Seghedi I (1998) Miocene acidic explosive volcanism in the Bükk Foreland, Hungary: Identifying eruptive sequences and searching for source locations. . Acta Geologica Hungarica 41:413-435

Széky-Fux V, Kozák M, Püspöki Z (2007) Covered Neogene volcanism of East Hungary. . Acta Geographica ac

Geologica et Meteorologica Debrecina, Geology, Geomorphology, Physical Geography Series 2:79-104

Tagami T, Farley KA, Stockli DF (2003) (U–Th)/He geochronology of single zircon grains of known Tertiary eruption age. Earth and Planetary Science Letters 207(1–4):57-67

Tari G, Dövényi P, Horváth F, Dunkl I, Lenkey L, Stefanescu M, Szafián P, Tóth T (1999) Lithospheric structure of the Pannonian basin derived from seismic, gravity and geothermal data., in Durand, B., Jolivet, L., Horváth, F., and Séranne, M., eds., The Mediterranean Basins: Tertiary extension within the Alpine orogen. Geological Society, London, Special Publication 156:215-250.

Vazquez J, Reid M (2002) Time scales of magma storage and differentiation of voluminous high-silica rhyolites at Yellowstone caldera, Wyoming. Contrib Mineral Petrol 144(3):274-285

von Quadt A, Gallhofer D, Guillong M, Peytcheva I, Waelle M, Sakata S (2014) U-Pb dating of CA/non-CA treated zircons obtained by LA-ICP-MS and CA-TIMS techniques: impact for their geological interpretation. Journal of Analytical Atomic Spectrometry 29(9):1618-1629

Walker Jr BA, Miller CF, Lowery Claiborne L, Wooden JL, Miller JS (2007) Geology and geochronology of the Spirit Mountain batholith, southern Nevada: Implications for timescales and physical processes of batholith construction. Journal of Volcanology and Geothermal Research 167(1–4):239-262

Watson EB, Harrison TM (1983): Zircon saturation revisited: temperature and composition effects in a variety of crustal magma types. Earth and Planetary Science Letters 64(2): 295-304

Wiedenbeck M, AllÉ P, Corfu F, Griffin WL, Meier M, Oberli F, Quadt AV, Roddick JC, Spiegel W (1995) Three natural zircon standards for U-Th-Pb, Lu-Hf, trace element and REE analyses. Geostandards Newsletter 19(1):1-23

Williams IS (1998) U-Th-Pb geochronology by ion microprobe. Rev. Econ. Geol. 7:1-35

Wilson CJN, Charlier BLA (2009) Rapid rates of magma generation at contemporaneous magma systems, Taupo Volcano, New Zealand: Insights from U–Th model-age spectra in zircons. Journal of Petrology 50(5):875-907

Wotzlaw J-F, Schaltegger U, Frick DA, Dungan MA, Gerdes A, Günther D (2013) Tracking the evolution of large-volume silicic magma reservoirs from assembly to supereruption. Geology 41(8):867-870.

Wotzlaw J-F, Bindeman IN, Watts KE, Schmitt AK, Caricchi L, Schaltegger U (2014) Linking rapid magma reservoir assembly and eruption trigger mechanisms at evolved Yellowstone-type supervolcanoes. Geology 42(9):807-810.

Wotzlaw J-F, Bindeman IN, Stern RA, D'Abzac F-X, Schaltegger U (2015) Rapid heterogeneous assembly of multiple magma reservoirs prior to Yellowstone supereruptions. Scientific Reports 5: 14026.

Zelenka T, Póka T, Márton E, Pécskay Z (2004) A Tari Dácittufa Formáció típuszelvényének felülvizsgálata. MÁFI Évi Jelentés 2004-ről:73-84

Zimmerer MJ, McIntosh WC (2012) The geochronology of volcanic and plutonic rocks at the Questa caldera: Constraints on the origin of caldera-related silicic magmas. Geological Society of America Bulletin 124(7-8):1394-1408

Figure Captions

Fig. 1 The position of Bükkalja Volcanic Field (BVF) in the Carpathian-Pannonian Region and a simplified geological map (based on the maps and the distinction of the main volcanic units provided by Szakács et al. 1998, Harangi et al. 2005 and Less et al. 2005a; 2005b) of the study area with the sample sites.

Fig. 2 Stratigraphic sequence at Tibolddaróc with volcanological description and interpretation (after Lukács et al. 2009) and with the location of the studied samples. Td-A was interpreted as represents the Harsány ignimbrite (Lukács et al. 2009), whereas the Td-M is the part of the Bogács unit described by Czuppon et al. (2012). Abbreviations of size fractions: A=ash; L=lapilli; B=block

Fig. 3 Sequences of Szv-3 and Mn-2 boreholes with the studied samples. Stratigraphy and distinction of the volcanic tuff horizons are based on the former drilling core interpretations compiled from well log documents of the Hungarian Geological Survey. Note, different vertical scales

Fig. 4 CL textures of typical zircons of Td-A samples with the LA-ICP-MS ages (uncertainties are 1-3% rse reported in the Online Resource 1). Scale is 100 µm

Fig. 5 CL textures of typical zircons of Group H (Td-H, DEMNE-1, FN1) samples with the LA-ICP-MS ages (uncertainties are 1-3% rse reported in the Online Resource 1). Scale is 100 µm

Fig. 6 a Comparison of LA-ICP-MS spot ages and UNMIX results of chemically abraded (CA) and non-abraded zircons of Td-H and Td-A samples. No detectable difference can be found between them based on the youngest UNMIX age populations (denoted with bold numbers). These similarities are supported also by the weighted mean values as shown in Table 1. Note that the smaller uncertainties of the individual spot ages in Td-A is due to the different analytical setup, i.e. in this case trace elements were not measured simultaneously with the U/Pb isotope ratios. **b** Zircon LA-ICP-MS U-Pb spot ages with UNMIX ages (Td-J, Td-F, Td-E; youngest age populations in bold) of samples from Tibolddaróc section.

Fig. 7 Results of in-situ LA-ICP-MS U-Pb age dating with the probability density curves and the calculated UNMIX ages (youngest age populations in bold) of samples from Szv3 and Mn2 boreholes and DEMNE-1 and FN1 localities

Fig. 8 Trace element variation of Group-1 (Td-H, DEMNE-1, FN1) and Group-2 (Td-A, Td-E, Szv3-1) zircons. Further diagrams are found in the Online Resource 5

Fig. 9 Hf vs. Ti-in-zircon-temperature (T_{TiZ}) plot showing also the zircon saturation temperature (T^{sat}) range calculated from the in-situ glass shard and pumice glass compositions of the Tibolddaróc (Td-A; Group-2) and Demjén (DEMNE-1; Group H) samples. This suggests that the studied zircons could have crystallized from a cold (< 760 °C) crystal mush environment. Symbols as in Fig. 8.

Fig. 10 Th/U vs. Y diagram for the Group-1 and Group-2 zircons. They form two distinct trends. The Group-1 trend is more coherent, whereas there is a larger scatter along the Group-2 trend. The Group-1 zircons have systematically lower Y content at given Th/U ratio than those of Group-2. Symbols as in Fig. 8.

Fig. 11 Th vs. Th/Y ratio plot and chondrite (Sun and McDonough 1989) normalized rare earth element diagram for the pumices and bulk tuff samples of the studied volcanic units. The trace element composition as well as the rare earth element patterns are clearly distinct in the samples with Group-1 and Group-2 zircons.

Fig. 12 Comparison of the interpreted eruption ages with the magnetic polarity epochs (Gee and Kent, 2007) and the available magnetic polarity data (Márton and Pécskay 1998; Márton et al. 2007). The narrow magnetic polarity subchrons help to bracket the eruption ages and refines the age of CCW rotation event defined by Márton et al. (2007) and the change in the regional stress-field (Márton and Fodor 2005, Petrik et al. 2014, 2015)

Table captions

Table 1 Samples with GPS coordinates and information about the in-situ U-Pb analyses including the weighted mean ages which have little meaning

Table 2 Results of ID-TIMS measurements

Table 3 Results of (U-Th)/He measurements

Table 4 Comparison of the interpreted eruption ages derived from in-situ zircon U-Pb and (U-Th)/He ages

Figure 1

Click here to download Figure Figure_1.tif

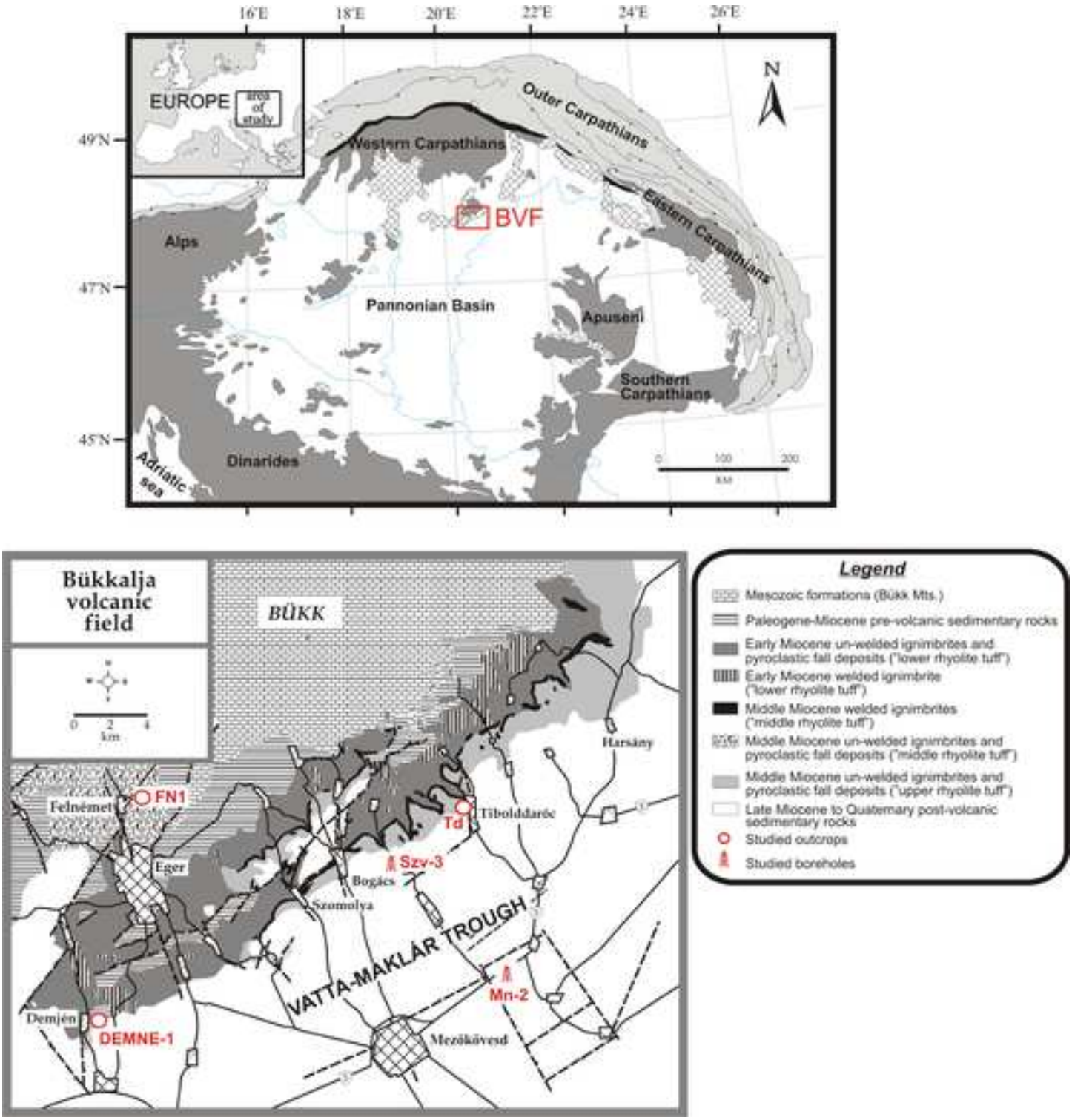

Figure 2

Click here to download Figure Fig_2_Td_section.tif

Tibolddaróc section (Bükkalja Volcanic Field)

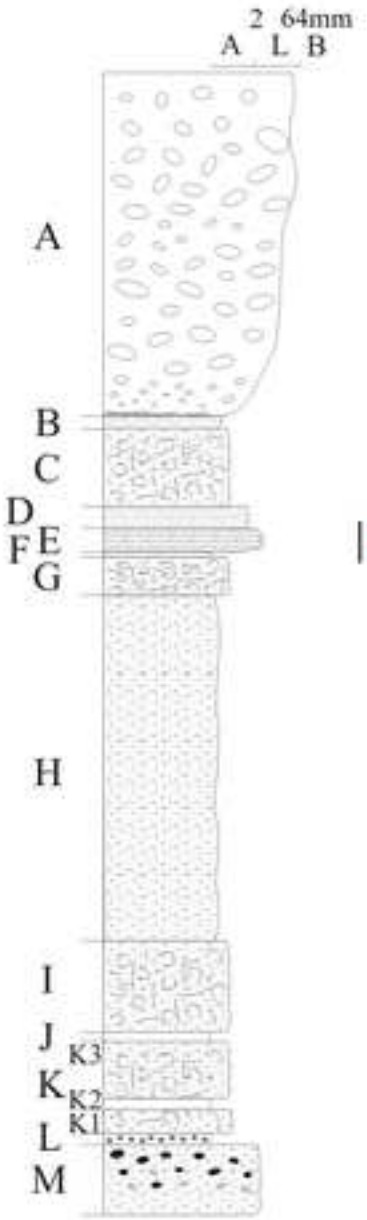

Sample name	Lithology	Genetic interpretation
Td-A (Harsány ignimbrite)	A: tuff - lapillituff - block-bearing lapillituff	pyroclastic flow deposit (ignimbrite)
	B: lapillituff	pyroclastic flow deposit
	C: reworked volcano-clastics	reworked volcano-clastics
	D: tuff	fall deposit
Td-E; Td-F	E: lapillituff	pyroclastic flow deposit
	F: fine tuff	fall deposit
	G: reworked volcano-clastics	reworked volcano-clastics
Td-H	H: lapilli-bearing tuff	ash-flow desposit
	I: reworked volcano-clastics	reworked volcano-clastics
	J: fine tuff	fall deposit
Td-J	K1; K3: reworked volcanoclastics	reworked volcano-clastics
	K2: fine tuff	fall deposit
	L: accretionary lapilli-bearing tuff	fall deposit
(Td-M: Bogács unit)	M: scoriae bearing lapillituff	pyroclastic flow deposit

Figure 3

Click here to download Figure Fig_3_boreholes_sections.TIF

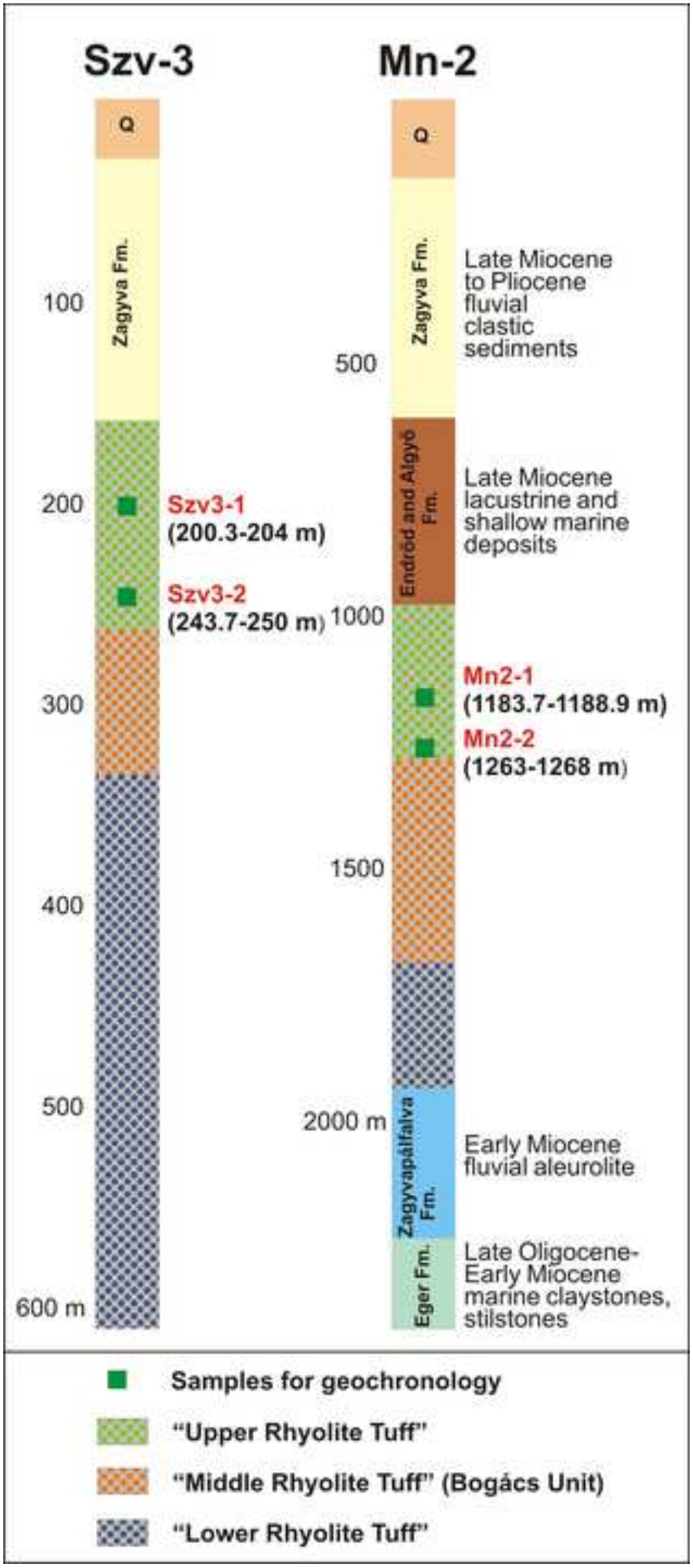

Figure 4

Click here to download Figure Fig_4_CL_Td_A.tif

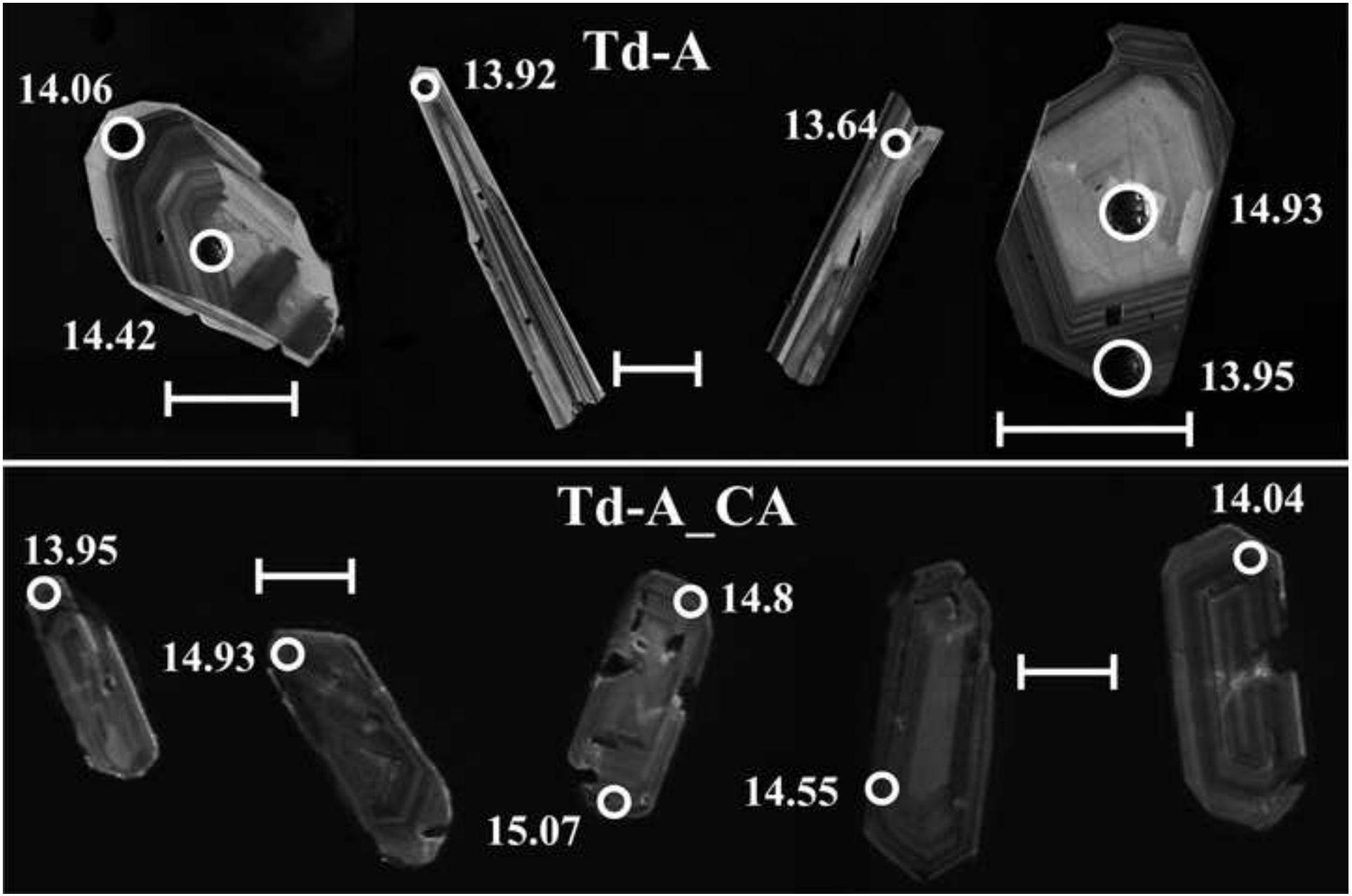

Figure 5

Click here to download Figure Fig_5_CL_Td_H.tif

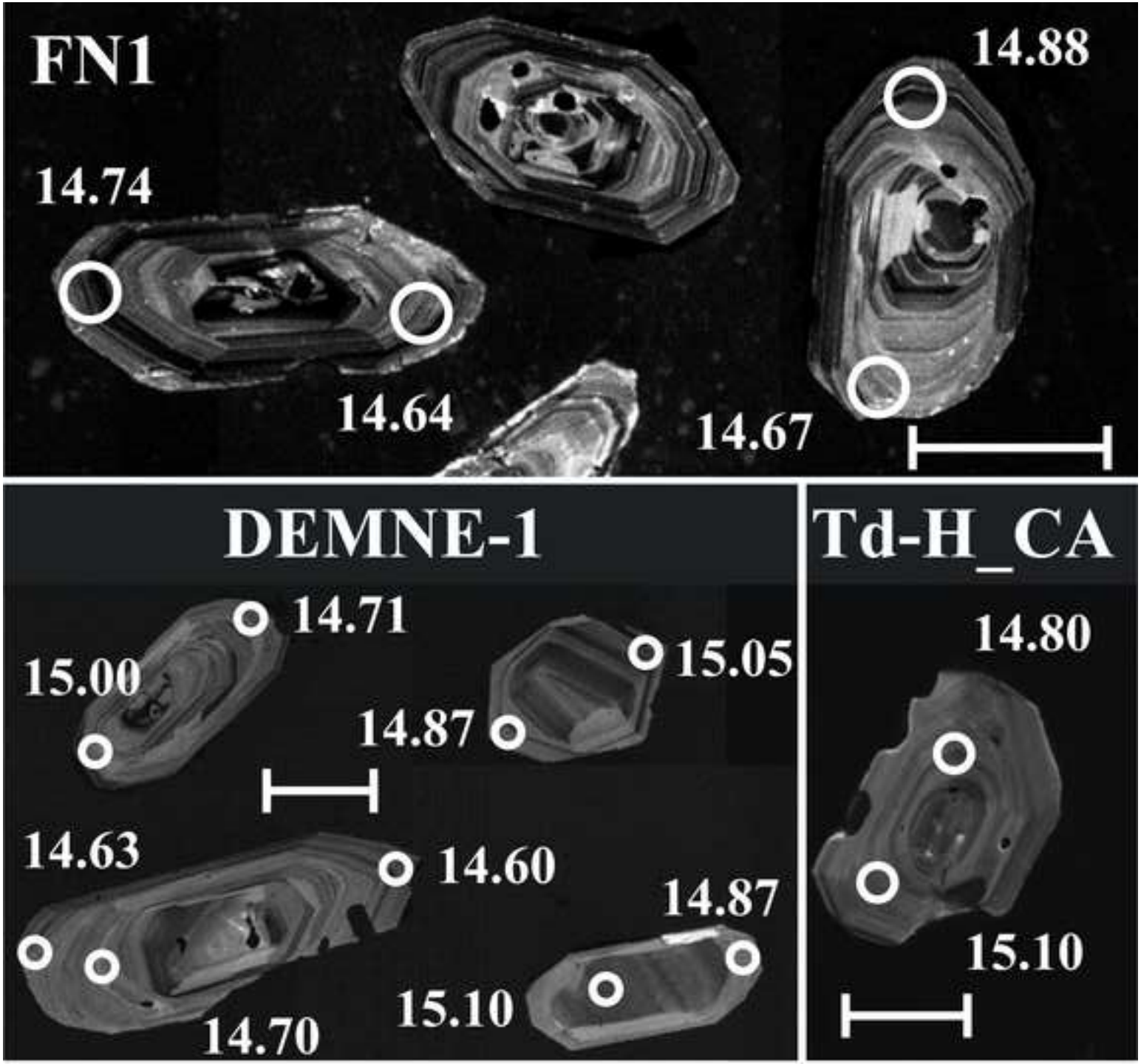

Figure 6

Click here to download Figure Figure_6.JPG

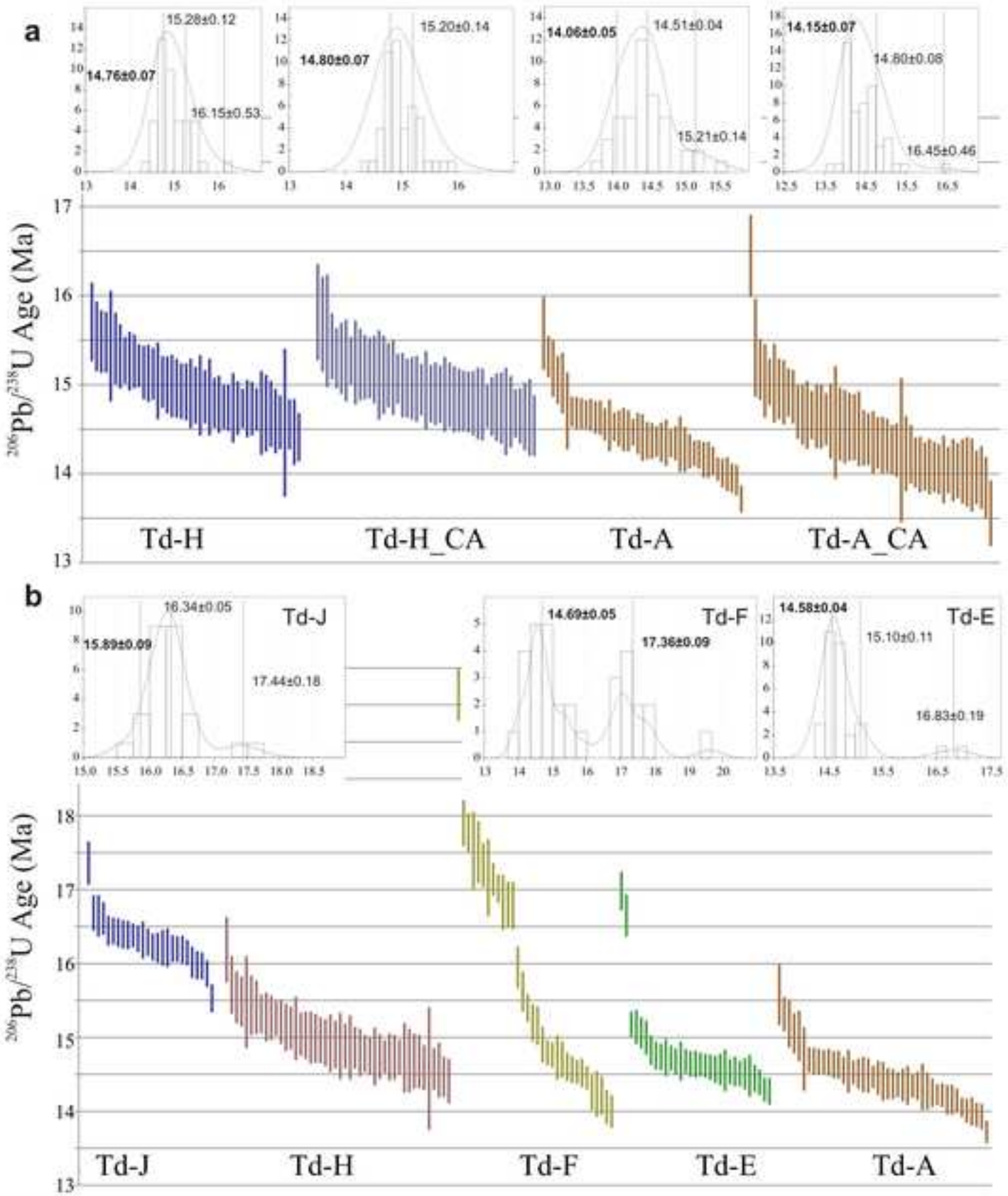

Figure 7

Click here to download Figure Figure_7.JPG

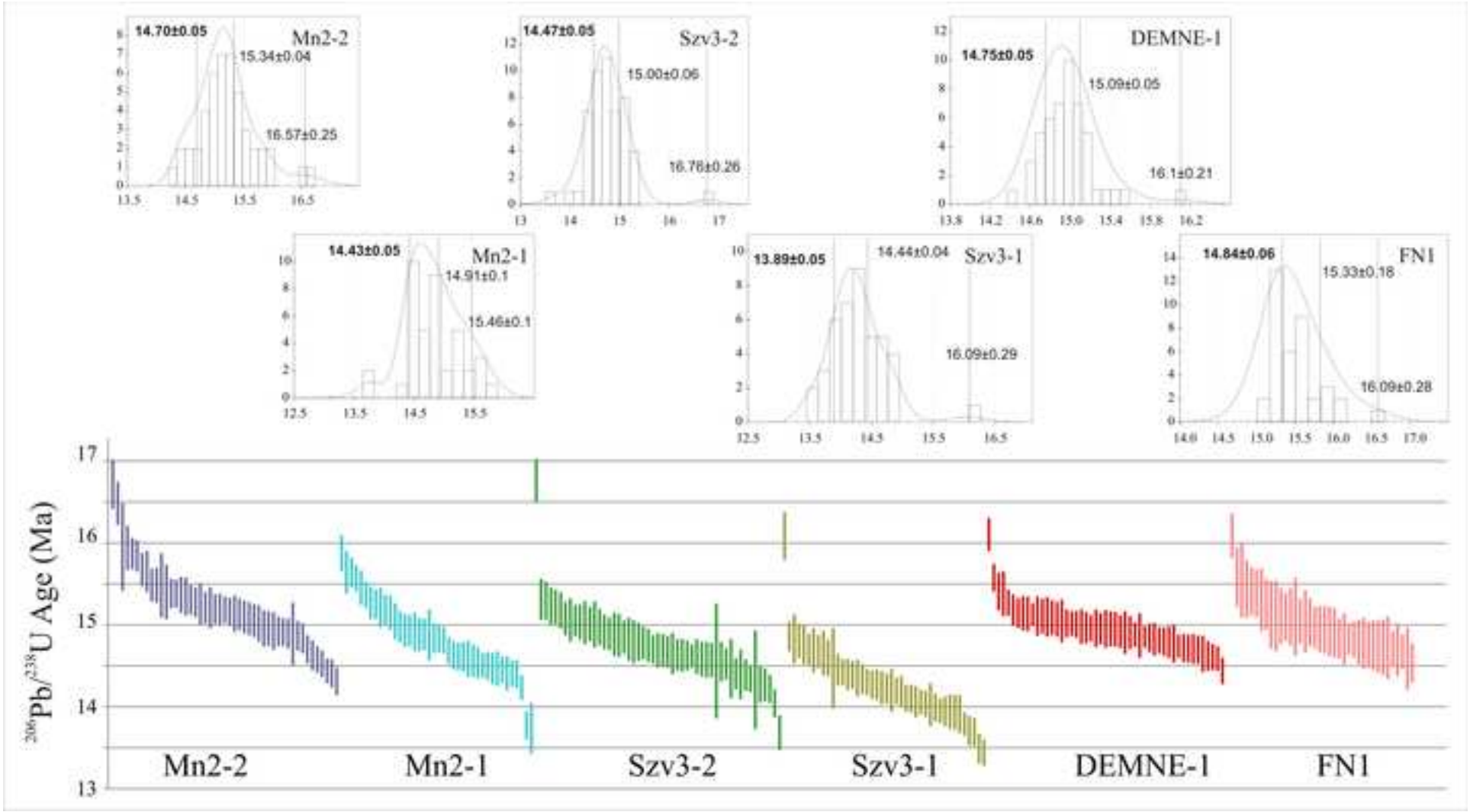

Figure 8

Click here to download Figure Figure_8.tif

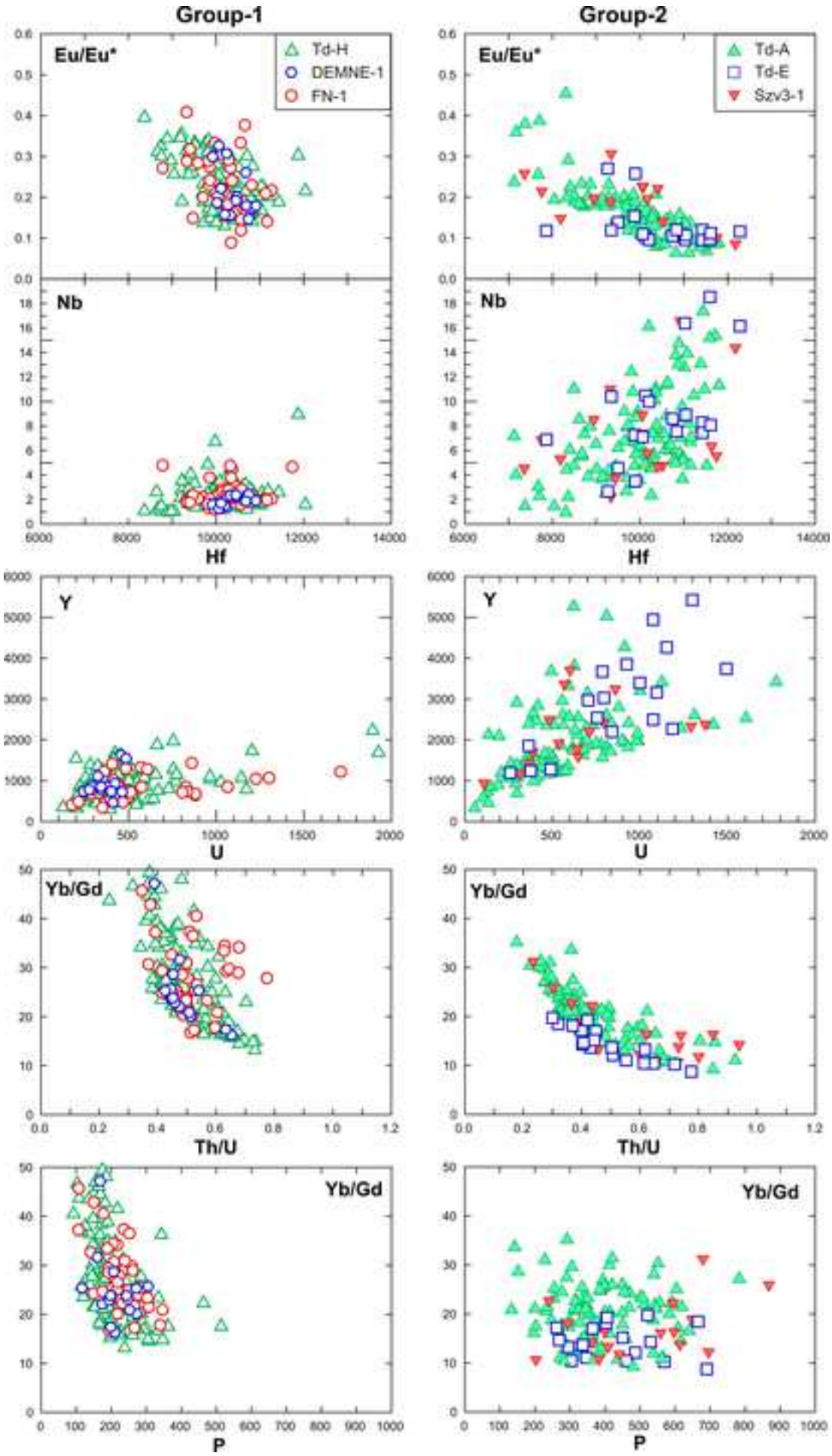

Figure 9

Click here to download Figure Figure_9.tif

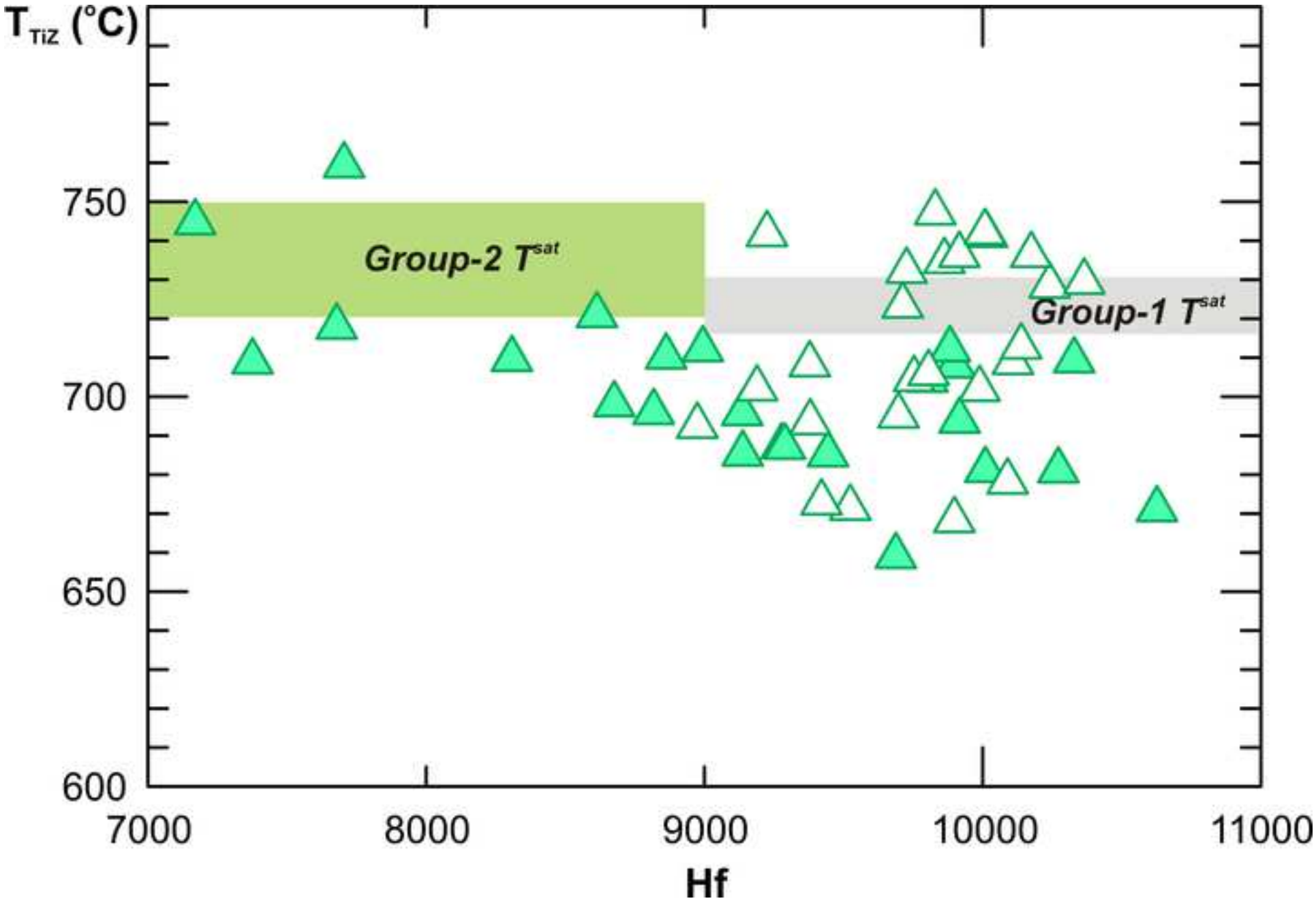

Figure 10

Click here to download Figure Figure_10.tif

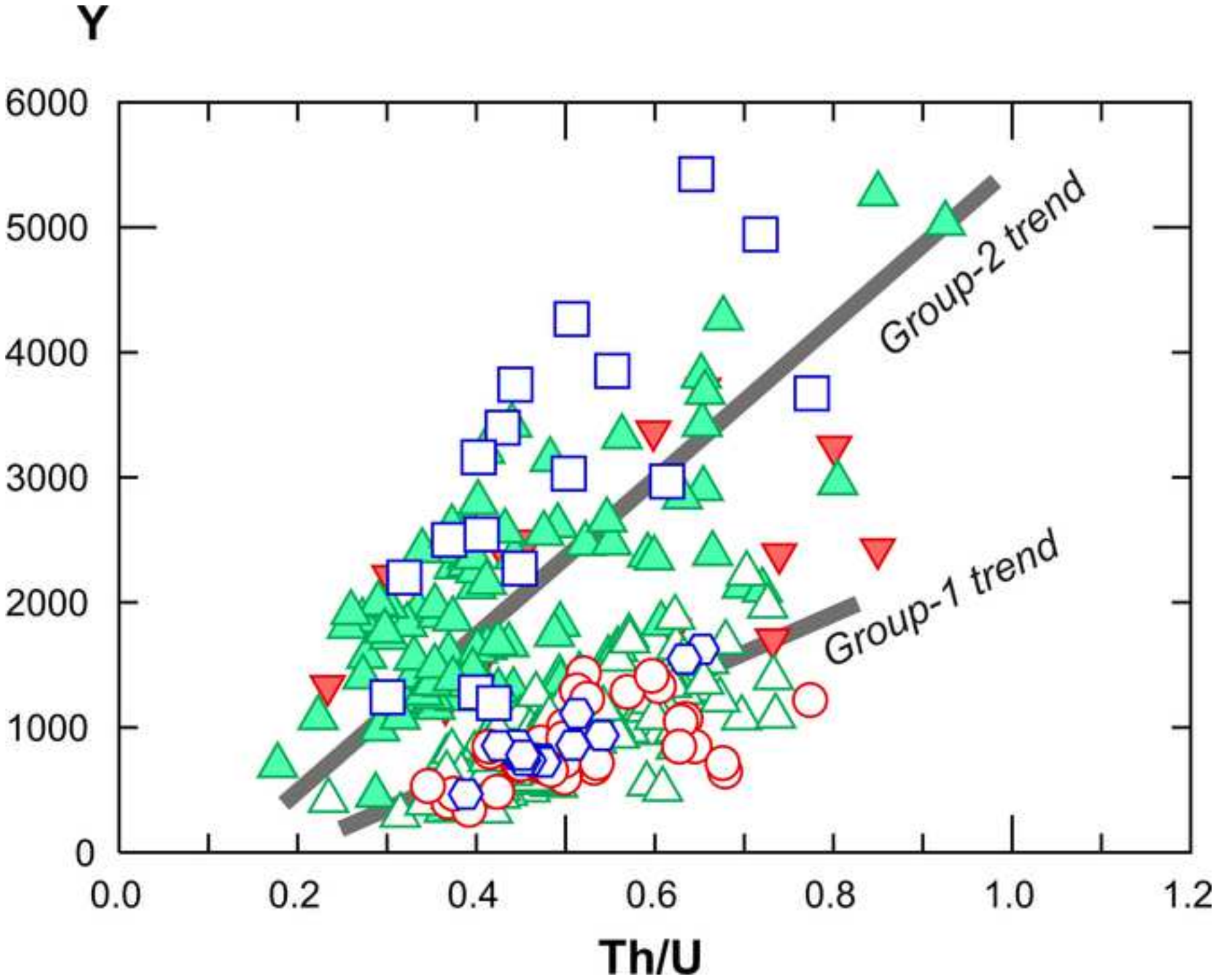

Figure 11

Click here to download Figure Figure_11.tif

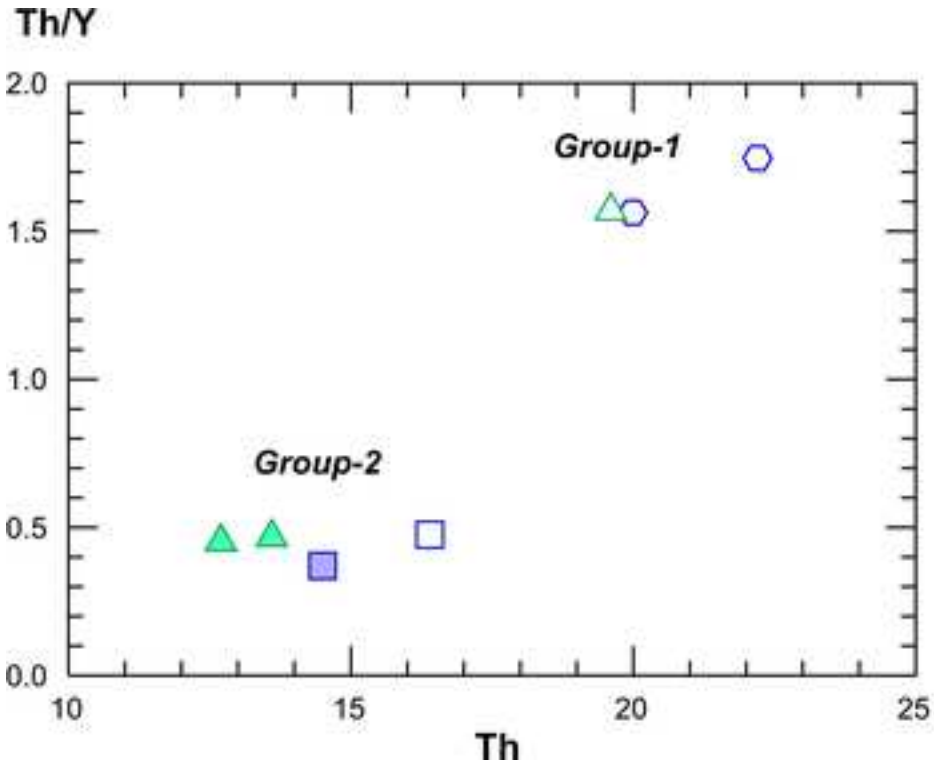

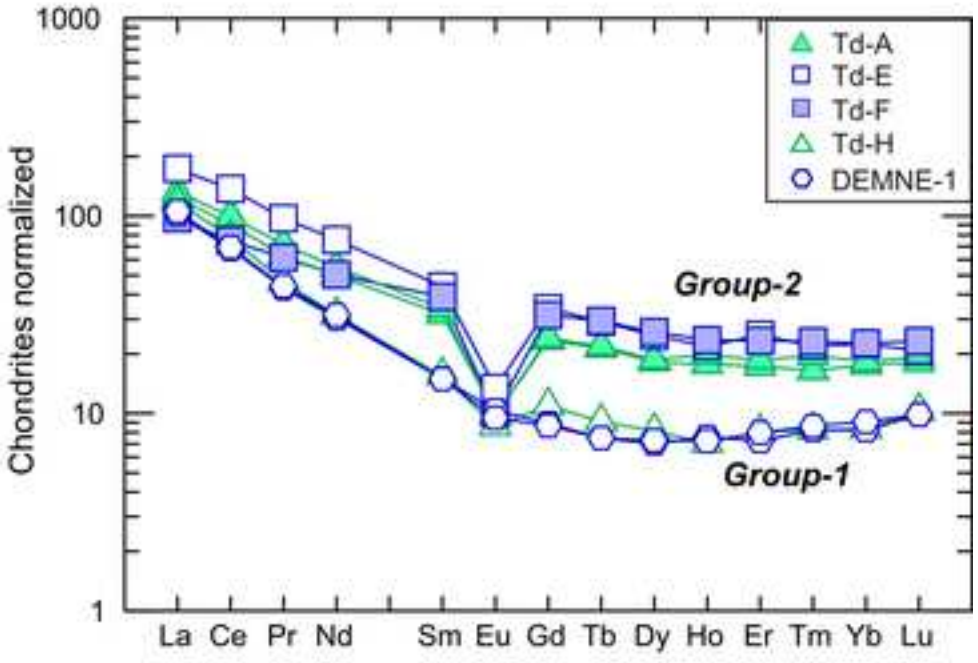

Figure 12

Click here to download Figure Figure_12.tif

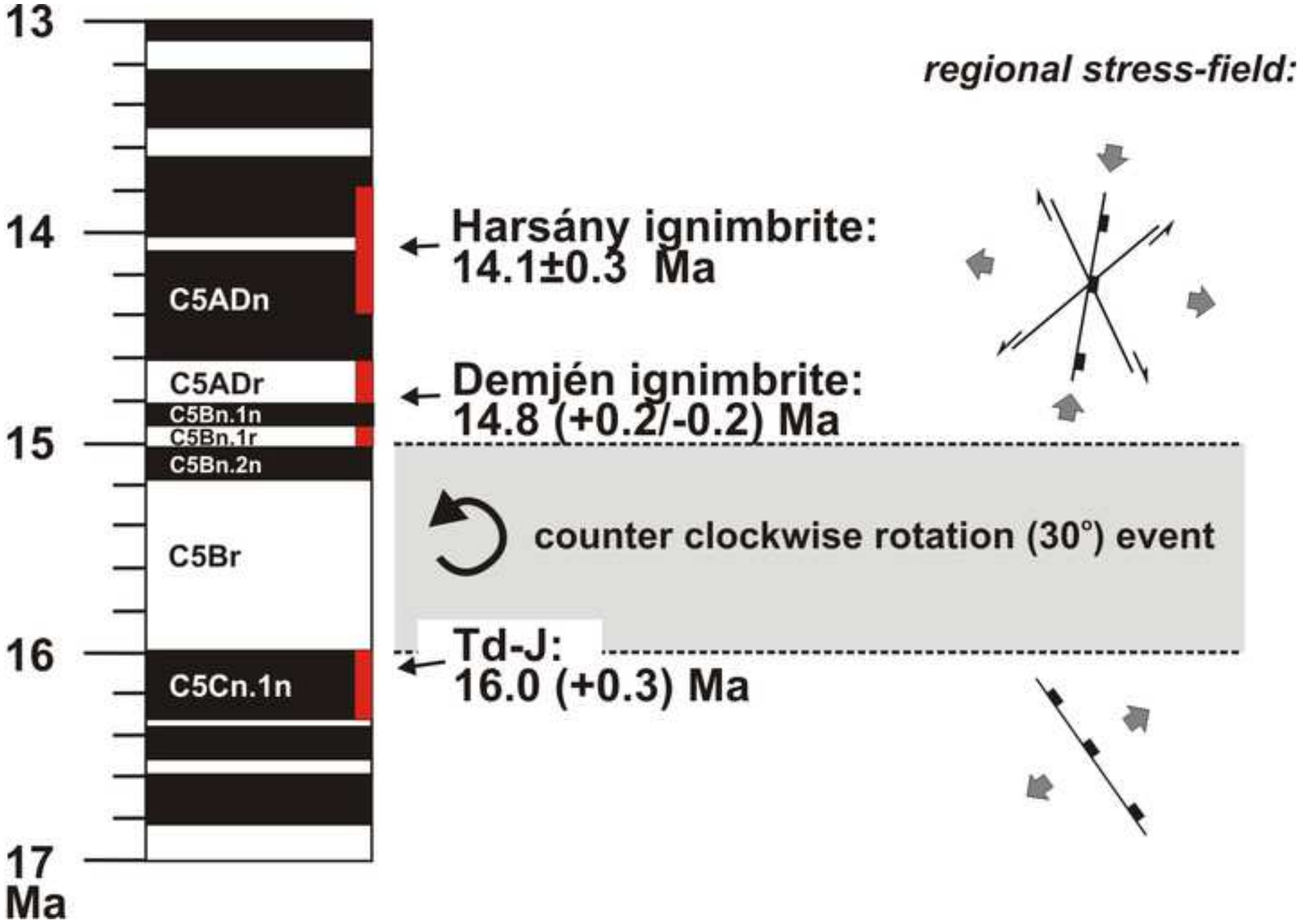

Table 1

Click here to download Table Table1.xls

Sample	GPS coordinates of sample localities	No. of analyses	No. of data taken to calculate wtd. mean[a], MSWD[a] and UNMIX	No. of outlier data (based on 2-sigma criteria)	Weighted mean age[a] (Ma ±2SE)	MSWD[a]	MSWD[b]	Average rse (%)
Td-J	**47°55'36.01"N, 20°37'57.65"E**	61	27	1 (Y) +2 (O)	16.23 ± 0.14	13	4.3	1.2
Td-H	**47°55'33.45"N, 20°37'55.55"E**	60	46	2 (O)	14.95 ± 0.10	4.1	3.2	2.3
Td-H_CA		50	48	2 (O)	14.92 ± 0.08	2.3	1.6	2.5
Td-E	**47°55'36.64"N, 20°37'55.19"E**	50	31	2 (O)	14.71 ± 0.16	22	5.4	1.3
Td-F		63	32	1 (O) +1 (P)				1.7
Td-A	**47°55'31.59"N, 20°37'49.77"E**	61	43	1 (Y) +3 (O)	14.37 ± 0.10	11.5	7.4	1.5
Td-A_CA		54	52	1 (O)	14.41 ± 0.12	6.5	5	2.5
Szv3-1	**47°54'11,46"N, 20°34'19,99"E**	70	42	1 (O)	14.19 ± 0.12	18	14	1.4
Szv3-2		65	51	1 (Y) +1 (O)	14.71 ± 0.11	15	8.1	1.6
Mn2-1	**47°51'16.49"N, 20°39'32.57"E**	67	40	2 (Y) + 1 (O)	14.80 ± 0.14	24	17	1.3
Mn2-2		58	47	2 (O)	15.10 ± 0.13	21	16	1.4
DEMNE-1	**47°50'1.58"N, 20°20'36.11"E**	52	49	2 (O)	14.94 ± 0.08	8.8	4.9	1.3
FN1	**47°56'0.29"N, 20°22'58.33"E**	50	37	1 (O) +1 (P)	14.96 ± 0.11	4.8	2.9	2.1

Y= younger outlier data; O= older outlier data; P= Proterozoic age data

[a] calcualted from data sets including outliers

[b] without outliers

Table 2 Click here to download Table Table2.xls

	Composition				Isotopic Ratios			
Sample	Th/U [a]	Pb*(pg) [b]	Pb_c(pg) [c]	Pb*/Pbc [d]	$^{206}Pb/^{204}Pb$ [e]	$^{206}Pb/^{238}U$ [f]	±2σ %	$^{207}Pb/^{235}U$ [f]
Td-A-z01	0.45	17.1	1.57	11	686	0.002223	0.07	0.01435
Td-A-z02	0.72	5.7	0.88	6	387	0.002220	0.08	0.01422
Td-A-z03	0.39	14.4	0.90	16	1011	0.002224	0.06	0.01441
Td-A-z04	0.92	6.5	1.00	6	369	0.002223	0.12	0.01438
Td-A-z05	0.44	15.2	1.36	11	707	0.002223	0.11	0.01435
Td-A-z06	0.43	6.1	1.07	6	369	0.002227	0.11	0.01461

[a] Th contents calculated from radiogenic ^{208}Pb and the $^{207}Pb/^{206}Pb$ date of the sample, assuming concordar

[b] Total mass of radiogenic Pb.

[c] Total mass of common Pb.

[d] Ratio of radiogenic Pb (including ^{208}Pb) to common Pb.

[e] Measured ratio corrected for fractionation and spike contribution only.

[f] Measured ratios corrected for fractionation, tracer and blank.

[g] Corrected for initial Th/U disequilibrium using radiogenic ^{208}Pb and Th/U_{magma} = 3

[h] Isotopic dates calculated using the decay constants λ^{238} = 1.55125E-10 and λ^{235} = 9.8485E-10 (Jaffey et a

				Dates (Ma)				
±2σ %	$^{207}Pb/^{206}Pb$ [f]	±2σ %	Corr. coef.	$^{206}Pb/^{238}U$ [g]	±2σ abs	$^{207}Pb/^{235}U$ [h]	±2σ abs	$^{207}Pb/^{206}Pb$ [g]
1.15	0.04683	1.14	0.152	14.406	0.011	14.46	0.16	23.9
2.08	0.04646	2.07	0.079	14.380	0.013	14.33	0.30	6.6
0.77	0.04701	0.76	0.140	14.419	0.008	14.53	0.11	33.0
2.16	0.04694	2.15	0.129	14.388	0.018	14.50	0.31	32.6
1.16	0.04685	1.15	0.152	14.409	0.016	14.47	0.17	24.9
2.13	0.04760	2.12	0.127	14.431	0.016	14.72	0.31	62.9
			average	**14.405**	**0.014**			
		weighted average		**14.408**	**0.018**	**MSWD=7.5**		

nce between U-Th and Pb systems.

l. 1971).

±2σ abs
27.3
49.9
18.3
51.5
27.6
50.5

Table 3

Click here to download Table Table3.xls

Sample code	232Th (ng)	Th error (%)	238U (ng)	U error (%)	147Sm (ng)	Sm error (%)	He (ncc)	He error (%)	TAU (%)	Th/U	Raw age (Ma)	±1σ (Ma)	Ft	Cor. age (Ma)	±1σ (Ma)	±1σ %
Td-H-1	2.131	2.3	4.085	2.5	0.003	12.6	6.328	1.2	2.5	0.52	11.3	0.3	0.81	**14.1**	**0.8**	**5.6**
Td-H-2	1.614	2.3	3.176	2.5	0.002	10.4	5.113	1.3	2.6	0.50	11.8	0.3	0.80	**14.7**	**0.8**	**5.6**
Td-H-3	1.217	2.3	2.424	2.5	0.003	12.1	3.512	1.2	2.6	0.50	10.6	0.3	0.77	**13.9**	**0.8**	**5.6**
Td-H-4	1.599	2.3	2.706	2.5	0.007	7.9	4.612	1.2	2.5	0.59	12.3	0.3	0.81	**15.2**	**0.9**	**5.6**
Td-H-5	1.100	2.3	2.336	2.5	0.002	10.8	3.658	1.4	2.7	0.47	11.6	0.3	0.79	**14.7**	**0.8**	**5.7**
Td-H-6	2.438	2.3	4.088	2.5	0.011	4.3	7.097	1.4	2.6	0.59	12.5	0.3	0.83	**15.0**	**0.8**	**5.7**
Td-H-7	0.896	2.3	1.209	2.5	0.002	11.5	2.005	1.4	2.6	0.74	11.6	0.3	0.77	**15.0**	**0.8**	**5.6**
											Weighted average +/- 2 sigma:			**14.63**	**0.61**	**4.2**
Td-A-1	1.004	1.4	2.048	1.9	0.004	8.2	3.333	1.2	2.1	0.49	12.0	0.2	0.79	**15.2**	**0.8**	**5.4**
Td-A-2	1.531	1.9	3.468	2.4	0.013	4.4	4.687	1.2	2.4	0.44	10.1	0.2	0.72	**14.0**	**0.8**	**5.6**
Td-A-3	1.027	1.4	1.653	1.9	0.006	7.9	2.447	1.4	2.1	0.62	10.6	0.2	0.73	**14.5**	**0.8**	**5.4**
Td-A-4	0.898	1.4	1.641	1.9	0.008	5.3	2.471	1.2	2.0	0.54	11.0	0.2	0.76	**14.4**	**0.8**	**5.4**
Td-A-5	1.397	1.4	3.066	1.9	0.008	4.9	3.957	1.3	2.1	0.45	9.6	0.2	0.69	**13.9**	**0.8**	**5.4**
Td-A-6	1.602	1.4	2.221	2.0	0.009	6.4	3.489	1.2	2.1	0.72	11.0	0.2	0.78	**14.1**	**0.8**	**5.4**
Td-A-7	1.186	1.4	3.246	1.9	0.005	7.7	3.939	1.2	2.1	0.36	9.2	0.2	0.66	**13.9**	**0.8**	**5.4**
											Weighted average +/- 2 sigma:			**14.27**	**0.59**	**4.1**
Szv-3-1-1	6.967	1.5	12.138	2.0	0.011	6.4	18.748	1.2	2.1	0.57	11.2	0.2	0.77	**14.5**	**0.8**	**5.4**
Szv-3-1-2	1.433	1.5	3.368	1.9	0.022	4.9	4.759	1.7	2.4	0.42	10.6	0.3	0.78	**13.6**	**0.8**	**5.6**
Szv-3-1-3	1.089	1.5	2.098	1.9	0.010	6.8	3.149	2.1	2.7	0.52	11.0	0.3	0.80	**13.8**	**0.8**	**5.7**
Szv-3-1-4	1.098	1.5	3.438	1.9	0.008	6.0	4.596	1.7	2.5	0.32	10.2	0.3	0.78	**13.1**	**0.7**	**5.6**
Szv-3-1-5	1.053	1.5	2.272	1.9	0.010	6.2	3.657	1.9	2.6	0.46	11.9	0.3	0.80	**15.0**	**0.8**	**5.6**
Szv-3-1-6	1.224	1.5	2.738	1.9	0.034	3.6	4.256	1.8	2.5	0.44	11.6	0.3	0.78	**14.8**	**0.8**	**5.6**
Szv-3-1-7	2.801	2.1	6.584	2.4	0.018	4.4	9.916	1.3	2.6	0.42	11.2	0.3	0.74	**15.2**	**0.9**	**5.6**
											Weighted average +/- 2 sigma:			**14.19**	**0.60**	**4.2**
Mn-2-1-1	1.360	1.5	3.258	1.9	0.004	9.9	4.551	1.7	2.4	0.41	10.5	0.3	0.71	**14.7**	**0.8**	**5.6**
Mn-2-1-2	1.348	1.5	2.948	1.9	0.001	20.4	3.915	1.8	2.5	0.45	9.9	0.3	0.69	**14.3**	**0.8**	**5.6**
Mn-2-1-3	2.270	1.5	3.402	2.0	0.003	10.5	5.053	1.6	2.3	0.66	10.5	0.2	0.75	**14.1**	**0.8**	**5.5**
Mn-2-1-4	2.375	1.5	3.748	1.9	0.002	16.7	6.066	1.5	2.3	0.63	11.6	0.3	0.76	**15.2**	**0.8**	**5.5**
Mn-2-1-5	1.252	1.5	1.760	1.9	0.002	13.2	2.633	2.3	2.9	0.71	10.5	0.3	0.74	**14.2**	**0.8**	**5.8**
Mn-2-1-6	0.859	1.5	2.310	1.9	0.005	6.8	2.910	2.2	2.8	0.37	9.5	0.3	0.67	**14.3**	**0.8**	**5.7**
											Weighted average +/- 2 sigma:			**14.45**	**0.66**	**4.6**
Mn-2-2-1	2.013	1.5	4.386	1.9	0.008	5.9	6.581	1.4	2.2	0.46	11.1	0.2	0.79	**14.2**	**0.8**	**5.5**
Mn-2-2-2	3.577	1.5	6.666	1.9	0.012	4.7	5.382	1.4	2.2	0.53	5.9	0.1	0.71	**8.2**	**0.5**	**5.5**
Mn-2-2-3	2.709	1.5	5.225	1.9	0.022	4.2	3.925	1.4	2.2	0.51	5.5	0.1	0.70	**7.8**	**0.4**	**5.5**
Mn-2-2-4	3.534	1.5	7.603	1.9	0.011	5.2	5.454	1.4	2.2	0.46	5.3	0.1	0.70	**7.5**	**0.4**	**5.5**
Mn-2-2-5	3.555	1.5	7.098	1.9	0.034	2.8	9.301	1.4	2.2	0.50	9.6	0.2	0.76	**12.7**	**0.7**	**5.5**
Mn-2-2-6	3.232	1.5	7.302	1.9	0.011	4.7	8.497	1.4	2.2	0.44	8.7	0.2	0.74	**11.6**	**0.6**	**5.5**
Mn-2-2-7	4.797	1.5	12.141	1.9	0.008	7.0	7.483	1.4	2.3	0.39	4.6	0.1	0.68	**6.8**	**0.4**	**5.5**
											Weighted average +/- 2 sigma:			**n / a**		

Table 4 Click here to download Table Table4.xls

Samples	Geochemical Groups	Eruption units	interpretative eruption ages of in-situ U-Pb dating (Ma)	final 2 sigma error[a]
Tibolddaróc section samples				
Td-J		Td-J Unit	15.9	0.3
Td-H	Group-1	Demjén Ignimbrite	14.8	0.3
Td-E	Group-2	Unit of Td-E and Td-F	14.6	0.3
Td-F	Group-2		14.7	0.3
Td-A	Group-2	Harsány Ignimbrite	14.1	0.3
Borehole samples				
Szv3-1	Group-2	Harsány Ignimbrite	13.9	0.3
Szv3-2		not defined	14.5	0.3
Mn2-1		not defined	14.4	0.3
Mn2-2		not defined	14.7	0.3
West BVF samples				
DEMNE-1	Group-1	Demjén Ignimbrite	14.8	0.3
FN1	Group-1	Demjén Ignimbrite	14.8	0.3

[a] including propagated external errors
n.d.= not determined

(U-Th)/He age (Ma)	2 sigma error
n.d.	
14.6	0.6
n.d.	
n.d.	
14.3	0.6
14.2	0.6
n.d.	
14.5	0.7
not available	
n.d.	
n.d.	